Luís Gonçalo Moreira Araújo

Bachelor in Micro and Nanotechnologies Engineering

ZnO nanoparticles as a potential biolabel for bioimaging applications

Dissertation submitted in partial fulfillment of
the requirements for the degree of

Master of Science in
Micro and Nanotechnologies Engineering

Adviser: Dr. Elvira Fortunato, Full Professor, Faculty of Science and Technology, NOVA University of Lisbon

Co-advisers: Dr. Ana Pimentel, Researcher, Faculty of Science and Technology, NOVA University of Lisbon

Examination Committee

Chair: Dr. Rodrigo Ferrão de Paiva Martins, Full Professor, NOVA University of Lisbon

Rapporteurs: Dr. Rita Maria Mourão Salazar Branquinho, Assistant Professor, NOVA University of Lisbon

Member: Dr. Ana Cláudia Madeira Botas Gomes Pimentel, Researcher, NOVA University of Lisbon

June 2021

FACULDADE DE CIÊNCIAS E TECNOLOGIA
UNIVERSIDADE NOVA DE LISBOA

ZnO nanoparticles as a potential biolabel for bioimaging applications

“Now is the time to understand more, so that we may fear less.”

– **Marie Curie**

Acknowledgments

I would like to thank all of those who helped me through these challenging years, which culminated in this dissertation.

I start by thanking my advisor, Prof. Dr. Elvira Fortunato, to my co-advisor, Dr. Ana Pimentel and to Ana Carolina Marques for all the help, monitoring and guidance they have been giving me throughout this dissertation, as well as for the opportunity to work on this topic.

I would also like to thank the rest of the CENIMAT|i3N team and thesis colleagues for all the help, sympathy and patience shown over this period.

To the PhD professors Joana Rodrigues and Teresa Monteiro from the physics department of the University of Aveiro, I am also very grateful for the collaboration through the tests and analysis carried out, which allowed a better understanding of the work done.

I thank Dr. Bruno Costa-Silva and the Champalimaud foundation for their interest in collaborating with this project.

To all the teachers that I have had throughout this course, and in particular, to the professors of the Department of Material Sciences, I thank you for always showing your willingness to help when necessary.

I would also like to thank Prof. Dr. Rodrigo Martins and Prof. Dr. Elvira Fortunato for the creation of the micro and nanotechnologies engineering course and for the concern in providing the best working conditions to the students.

I also thank the DCM and CENIMAT|i3N secretariat for all the help and availability given during this work.

A todos os colegas e amigos ganhos ao longo destes anos, de forma mais ou menos direta através da universidade, devo também um grande agradecimento por toda a entreajuda, amizade e momentos de descontração. Sem a vossa ajuda este percurso teria sido muito mais difícil (se é que possível). Agradeço em especial ao Rui, Tiago, Violas e à Célia por todos os momentos de confraternidade e estudo passados ao longo destes anos.

Aos meus pais, palavras não chegam para exprimir a minha gratidão, sem vocês não estaria aqui (nem em qualquer outro lugar), muito obrigado por tudo! E vá, agradeço também à minha irmã Rita por ser uma boa maninha mais nova (embora um bocadinho chata, às vezes).

Aos meus avós e restante família, um grande obrigado por todos os ensinamentos, apoio e carinho que sempre me foram dados de forma incondicional.

Ao Pedro, Inês, Rui, Violas e Célia agradeço também a ajuda com a revisão deste trabalho (assim como por tudo o resto).

Por último, agradeço também a todos os que me deram cebolas, para a realização de experiências, quando me esquecia destas.

A todos, uma vez mais, muito obrigado!

Abstract

In order to better understand biological processes and thus understand and find better treatments for diseases, it is essential to have suitable bioimaging methods. One of these methods is confocal microscopy, which uses fluorescence. To confer fluorescence and thus study biological samples, many different types of fluorophores can be used.

One of these types of fluorophores are nanoparticles, which have several advantages in comparison with other fluorophores. However, the nanoparticles most traditionally used for obtaining biological images use cadmium, which is very toxic. For this reason, different materials have been studied in order to conceive nanoparticles with high fluorescence and low toxicity, of which zinc oxide (ZnO) nanoparticles have generated considerable interest because, in addition to their good optical properties, these are also considered safe, being used in various areas and products such as sunscreens, cosmetics, and food packaging. Moreover, the ZnO nanoparticles are still very promising in medicine to be used in the fight against cancer and have antibacterial properties.

However, as ZnO nanoparticles have a high band gap, their fluorescence mainly occurs when they are irradiated with low wavelengths, which are not commonly used in confocal microscopy or in biological samples. Due to this, throughout this thesis, ways of increasing the fluorescence of ZnO nanoparticles (by using longer wavelengths) will be studied, namely by doping them with europium, as well as the effects that different syntheses/doping concentrations influence other properties of these nanoparticles (such as morphology and crystallinity). To finalize, the fluorescence conferred to biological samples through the use of the synthesized nanoparticles will also be analyzed through confocal microscopy. The obtained results were compared with those obtained with a commercial fluorophore.

Keywords: ZnO nanoparticles, Solvothermal, Europium, Fluorescence, Bioimaging

Resumo

De forma a melhor entender processos biológicos, e assim perceber e encontrar melhores tratamentos para doenças, é muito importante ter bons métodos para a obtenção de imagens biológicas. Um desses métodos é através de microscopia confocal a qual usa fluorescência. Para conferir fluorescência e assim estudar amostras biológicas, há muitos tipos diferentes de fluoróforos que podem ser usados.

Um desses tipos de fluoróforos são nanopartículas as quais possuem várias vantagens em comparação com outros fluoróforos. No entanto, as nanopartículas mais utilizadas para a obtenção de imagens biológicas usam cádmio, apresentando uma elevada toxicidade. Por este motivo, outros materiais têm sido estudados de forma a ser possível obter nanopartículas com elevada fluorescência e baixa toxicidade, sendo o óxido de zinco (ZnO) bastante interessante pois, para além das suas boas propriedades óticas, as nanopartículas de ZnO são também consideradas seguras sendo usadas em diversas áreas e produtos como, protetores solares, cosméticos, e embalagens para comida. Para além disto, as nanopartículas de ZnO, mostram-se ainda muito promissoras em medicina para serem usadas na luta contra o cancro e apresentam propriedades antibacterianas.

No entanto, devido ao elevado band gap das nanopartículas de ZnO, a sua fluorescência ocorre principalmente quando estas são irradiadas com baixos comprimentos de onda, os quais, por norma, não são usados em microscopia confocal nem em amostras biológicas. Desta forma, ao longo desta tese serão estudadas formas de aumentar a fluorescência das nanopartículas de ZnO (para maiores comprimentos de onda), nomeadamente através da dopagem destas com európio, assim como os efeitos que diferentes sínteses/dopagens influenciam outras propriedades destas nanopartículas (como morfologia e cristalinidade). Por fim a fluorescência conferida a amostras biológicas através da utilização das nanopartículas sintetizadas será também analisada através microscopia confocal, tendo sido também comparadas as propriedades obtidas com as de um fluoróforo comercial.

Palavras-chave: Nanopartículas de ZnO, Solvo-térmica, Európio, Fluorescência, Bio-imagem.

Table of Contents

List of Figures

List of Tables

Abbreviations

CB - Conduction band

DLE - Deep Level Emission

DLS - Dynamic Light Scattering

DS - Defect states

EDXS - Energy Dispersive X-ray Spectroscopy

FITC - Fluorescein Isothiocyanate

FPs - Fluorophores

FWHM - Full Width at Half-maximum

NBE - Near Band Edge Emission

NPs - Nanoparticles

pa - Post-annealed

PL - Photoluminescence

PLE - Photoluminescence Excitation

RT - Room Temperature

SEM - Scanning Electron Microscopy

UV - Ultraviolet

Uv-Vis - Ultraviolet-Visible

VB - Valence band

XRD - X-ray Diffraction

Symbols

A – Energy independent constant used to calculate the band gap

D – Crystallite size length obtained from the analyzed peak

Eg – Band gap energy

G – Main gain used on confocal laser scanning microscopy

h – Planck constant

I – Intensity of the laser used on confocal laser scanning microscopy

k – Correlation factor used for Scherrer's equation related to the shape of the crystallite

M – Molar concentration

$R\infty$ – Reflectance of an infinitely thick specimen

α – Absorption coefficient

β – Full width at half-maximum of a peak (FWHM)

γ – Constant that depends on the nature of the electron transition used to calculate the band gap

θ – Bragg's diffraction angle

λ – Wavelength

ν – Photon's frequency

Motivation and Objectives

As recent times have shown, having viable methods to understand biological processes and their interactions is very important to acquire a better understanding of diseases and, thus, to find better treatments and cures.

One of these methods is fluorescence microscopy, which is a vital tool in life sciences, being the most common way to study dynamic cellular events. As the name indicates, this method uses fluorescence to obtain images of what is being analyzed. In most cases, it is necessary to confer fluorescence to the object in study through the use of fluorophores.

One of the types of fluorophores that can be used is nanoparticles, which have several advantages compared to other fluorophores, like higher brightness, higher photostability and the capability for carrying various sensing and therapeutic components. However, the nanoparticles most traditionally used in bioimaging are based on cadmium which is considered a highly toxic material. For this reason, nanoparticles that confer high fluorescence and low toxicity have been studied, from which zinc oxide nanoparticles have gained a lot of interest thanks to presenting several other advantages like anticancer properties.

However, due to the high band gap of ZnO nanoparticles, their fluorescence mainly occurs when irradiated with low wavelengths, which are not commonly used in biological samples and on confocal microscopy since it can damage the samples and has a low penetration in tissues.

In this way, the main objective of this work was the production of ZnO nanoparticles with fluorescence properties, when irradiated with wavelengths regularly used on confocal microscopy, i.e., higher than 400 nm, as well as nanoparticles with satisfactory morphologies to be used as fluorophores in biological cells and thus these should present a spherical shape with small diameters, so that they are more rapidly absorbed by most of the cells.

Work Structure

This dissertation is divided into four main parts: introduction, materials and methods, results and discussion, and conclusion.

In the introduction section, it will, initially, be given an overview on bioimaging, fluorescence microscopy and some of the most used fluorophores, with the latter being then explored in greater detail. Following that, the advantages and disadvantages that nanoparticles and, more specifically, ZnO nanoparticles have in comparison with other fluorophores will be analyzed. The introduction will be concluded by showing how it is possible to improve the fluorescence of the ZnO nanoparticles by doping them with europium.

The synthesis protocols used to produce the nanoparticles and some of the studied parameters will be described in the materials and methods chapter, as well as the main experimental details used to characterize the samples.

In results and discussion, a complete characterization of the different samples obtained through the various synthesis methods will be presented and analyzed. This part of the thesis is divided into the results that give mainly structural and morphological information and into the results concerning the optical properties, even though relations between these are expected.

Finally, the main results of this work will be summarized. There will also be given some general conclusions regarding the use of ZnO nanoparticles in bioimaging and some future work possibilities.

Annexes with additional information can also be found at the end of this dissertation.

1. Introduction

1.1 Bioimaging

In order to better understand diseases and to find their cures, it is highly relevant to use methods like bioimaging, which allows a non-invasive visualization of biological processes and structures in real-time. There are several bioimaging methods, such as computed tomography, magnetic resonance imaging, positron emission tomography, and fluorescence imaging. These methods present different advantages and therefore are used in various applications, being, for example, fluorescence microscopy a very useful tool to monitor cell physiology (in live cells). [1]

1.2 Fluorescence microscopy

As mentioned above, fluorescence microscopy has become a very useful tool to monitor cell physiology due to attributes usually not available in other optical microscopy modes (like the use of fluorescent indicators). In this way, fluorescence microscopy enables the detection and localization of a minimal number of molecules in biological samples and the investigation of the spatiotemporal dynamics of cells, tissues, and developing organisms. This lead to fluorescence microscopy becoming indispensable in life sciences and has potentially made live-cell fluorescence microscopy the most common way to study dynamic cellular events. [1]–[7]

In most cases, to perform fluorescent microscopy, it is necessary to incubate the samples with materials able to confer them fluorescence properties. These substances are called fluorophores (FPs) and their use allows the visualization of protein locations, to identify protein complex formation and changes in its shape and to monitor biological processes *in vivo*. This is possible by labeling the FPs through molecules such as protein, nucleic acid, and antibodies, being the FPs then used to detect (and mark) a specific target, i.e. to biolabel. [1]–[3], [8]

Fluorescence occurs when there is luminescence (emission of light by any other form than due to the temperature of a substance, i.e., incandescence) through the absorption of photons (photoluminescence). It differs from phosphorescent since fluorescence presents its emission almost immediately after excitation while, in phosphorescent, the absorbed energy can be stored for some time. In this way, so that fluorescence occurs, the fluorophore must be irradiated by a specific range of wavelengths, with sufficient energy to excite the electrons present on the FPs. This energy will be absorbed by electrons of the FPs, raising them to an excited state where some energy will be lost. The remaining energy will then be lost by the emission of photons of a longer wavelength (lower energy) than the excitation photons, being the emission light from the fluorophore of a different range of wavelengths than the excitation light (due to the loss of energy) (Figure 1.1). The difference between the excitation and emission energy is called Stokes-shift. [1]–[3], [8]–[10]

A special type of fluorescence microscopy is confocal microscopy and through this method, the beam used is focused in a small area of the sample that will be scanned, and the out-of-focus light can be rejected from the image through the use of a pinhole (Figure 1.1). Thanks to this, it is possible to divide the sample into different focal planes allowing to obtain 3D images. In addition, confocal microscopy offers other advantages, such as having fewer artifacts induced by tissue processing, making it a very important technique in several areas. [11], [12]

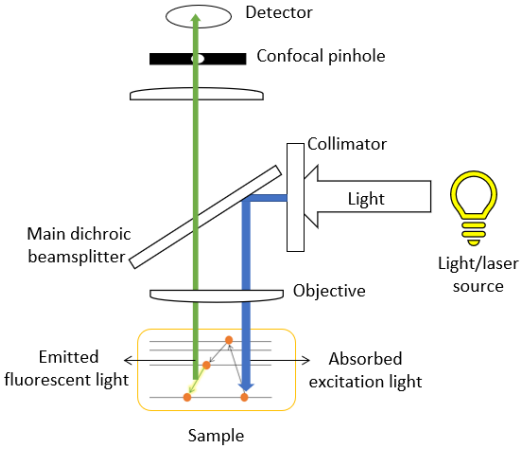

Figure 1.1 - Basic schematic of the light path in fluorescence microscopy and the changes in electron state during photon excitation and emission.[13]

1.3 Fluorophore types

FPs are the most important part of fluorescence microscopy since, ultimately, the obtained information from the experiment is determined by the properties of the FPs (like their brightness and photostability). Thousands of FPs are available, being possible to divide them into two main categories, intrinsic (like aromatic amino acids and flavins) and extrinsic FPs. Extrinsic FPs, opposite to intrinsic, are the FPs that are not present in the sample and thus must be added to confer luminescence to the sample. In this way, extrinsic FPs will be the ones that will be referred to throughout this dissertation. These FPs can be divided into many different types, such as classic organic dyes, lanthanide complexes, polymeric and dendrimeric dyes, metal-based dyes, fluorescent proteins, and nanoparticles. [14], [15]

Some important properties of the FPs are their probability of absorbing a photon (extinction coefficient); the ratio between the number of photons emitted by the PFs and the number of absorbed photons (quantum yield); stokes shift (difference in wavelength between the excitation and emission energy); and their brightness (extinction coefficient × quantum yield). The brightness of the FPs depends on several factors such as pH, temperature, and the intensity of the excitation light, being the brightness directly proportional to the intensity of the excitation light. However, high intensities of excitation light can lead to photobleaching of FPs, which is the irreversible loss of fluorescence ability, being a common issue in fluorescence imaging and thus, the used intensity must be considered as a relevant factor. Another phenomenon that decreases the fluorescence of the FPs is quenching, which happens when the electron does not emit light when returning to its stable state due to interactions with other molecules or other FPs. [6], [8], [15]

Some characteristics that ideal FPs must have are, high brightness, non-toxicity, low photobleaching, low cost, high stability, facile bio labeling and small size (in order to have less interference with biological processes). However, it is essential to notice that the ideal fluorophore varies from sample to sample according to its intended use. [6], [15]

1.3.1 Common Fluorophore Classes

From the previously mentioned FPs, fluorescent proteins and organic dyes are of the most used in fluorescence microscopy.

Most fluorescent proteins are derived from the jellyfish *Aequorea victoria* green fluorescent protein and have several advantages such as a broad spectral range, non-toxicity, and long lifetime. [6]

Organic dyes were the first fluorescent compounds used in biological research and thus, a lot is known about their properties. They present advantages, such as small size, facile bio labeling, easy availability, and broad spectral range. Fluorescein isothiocyanate (FITC) is one of the most commonly used FP. [6], [8], [15]

However, these FPs also have some disadvantages, like rapid photobleaching, low to medium brightness and small stokes shift. In this way, in cases like long-term tracking of single molecules and real-time super-resolution imaging of subcellular structures, FPs with higher brightness and higher photostability are needed to better understand cell physiology. [6], [8], [15], [16]

1.3.2 Nanoparticles

Thanks to advances in science and, more specifically, nanotechnology, the development of a great variety of nanoparticles (NPs) as FPs is possible. These NPs allow to overcome some of the disadvantages presented in other FPs, such as lower brightness, low photostability, and small stokes shift. In addition to these, they also offer advantages like tailorable surface modifications, capability for carrying various sensing and therapeutic components, low interaction with cellular proteins, detection at the single molecular level and real-time tracking of single biomolecules, making it possible to better understand some biological processes, not so well understood using other FPs. [6], [17]–[19]

Nanoparticles for fluorescence microscopy can be divided into two categories, which are the NPs that require labeling of FPs to be visualized and the NPs that can emit specific optical signals by themselves such as quantum, polymer and carbon dots, up-conversion-NPs, fluorescent nanodiamonds, and gold NPs [16], [18], [19]

Regarding the use of nanoparticles on cells and their interaction, while some organic dyes with specificity for cellular substructures can be small enough to be able to pass through the cell membrane, the higher dimensions of most NPs (> 5 nm) leads to these usually needing to enter the cells through mechanisms of cellular uptake. One of these mechanisms is clathrin-mediated endocytosis, which cells use to internalize ligand-conjugated NPs, being most of the NPs used for diagnostic and molecular imaging applications of this type. Thus, if the nanoparticles have a specific target inside the cell, more steps are needed to allow them to exit the vesicles and connect to their target. By using these mechanisms, the size and shape of NPs are two of the main factors that influence cellular uptake, being spherical NPs with a diameter of about 50 nm usually more rapidly absorbed by cells than other NPs. [16], [20]

Quantum dots are a special type of NPs characterized by their small size and for being semiconductors. Quantum dots are one of the most used NPs for biological labels as they are one of the most widely known nanoparticles to exhibit size-tunable features. In this way, it is possible to change their fluorescence emission and absorption wavelength by simply changing their particle size, whereas smaller quantum dots emit higher energy radiation. However, the most used quantum dots are cadmi-

um chalcogenides such as CdS, CdSe, and CdTe, which are toxic toward biological systems, being, in many cases, necessary to coat them with inert shells in order to present lower toxicity. In addition to this, cadmium chalcogenides also present lower long-term environmental stability, lower biocompatibility, and higher cost when compared with other NPs, such as ZnO NPs, making ZnO NPs of special interest to be used in bioimaging. [21], [22]

1.4 ZnO Nanoparticles

Metal oxide nanoparticles show promising prospects in several areas of the biomedical field from diagnostics, through their use on cell imaging and biosensing, to treatment, thanks to their antibacterial properties and for allowing anticancer drug/gene delivery. From these types of NPs, zinc oxide nanoparticles, ZnO NPs, are one of the most important, being extensively used in commercial products, such as paint, sunscreens, cosmetics, daily care products, food packages, and ointments. They are so extensively used due to having properties such as excellent biocompatibility, long-term environmental stability, low-cost production, and low toxicity. Furthermore, for having excellent luminescent properties, they become one of the more relevant candidates for bioimaging and possibly for theragnostic applications (that is, a combination of therapy and diagnostics). [23]–[25]

ZnO is a semiconductor material with a vast area of applications. Several techniques have been employed to study and improve the growth of ZnO nanostructures, which include electrospinning, precipitation, solvothermal, and even green synthesis methods by using plant extract, bacteria, fungi, etc. This variety of techniques allows the synthesis of ZnO nanostructures with different properties such as different sizes, crystallinities, and morphologies (nanorods, flower-like ZnO nanostructures, etc.). These differences in structural and morphological properties may influence other properties like biological interactions and optical properties. [20], [26]–[31]

The optical properties of ZnO NPs can be influenced by the crystallinity of these NPs since the fluorescence of the ZnO NPs originates mainly from surface defects, like oxygen vacancies. Highly crystalline ZnO NPs will present strong UV emission, while ZnO NPs with a high quantity of surface defects show high emission in the visible wavelength range. To obtain NPs with high emission in the visible wavelength range, sol-gel and wet chemical techniques are usually used due to lower synthesis temperatures allowing the presence of a higher number of ZnO surface defects. Thermal annealing is another parameter that can affect ZnO emissions. [20], [26]–[31]

As previously mentioned, in addition to using ZnO NPs for bioimaging, using this type of nanostructures as antibacterial material and for cancer treatment is also possible. This derives from the fact that, although being recognized as a safe material, ZnO NPs also have shown antibacterial properties through cytotoxic mechanisms like the accumulation of NPs in the outer membrane or cytoplasm of bacterial cells and the generation of reactive oxygen species (ROS). With respect to cancer treatment, thanks to ZnO being pH-responsive, dissolving in acid environments, they can be used in cancer therapy to deliver drugs to specific targeted tissues since the extracellular environment of solid tumors tissues is mildly acid. [32]

In this way, ZnO NPs have shown to be promising in both the fields of bioimaging and anticancer/antibacterial treatment. However, ZnO NPs still present some aspects to be improved and many studies are still needed to better understand ZnO NPs properties and how they can be successfully used in biomedical fields. One example of these is that the luminescence mechanisms and fluorescence lifetime of ZnO NPs are still not very well understood, being only a few methods able to im-

prove or change ZnO fluorescence effectively. Another example is the toxicity of ZnO NPs, which is still called into question due, in part, to their anticancer and antibacterial properties. [23], [32]

Another aspect that must be considered concerns the stability of ZnO NPs in water and biological fluids since surface defects of ZnO can be destroyed by water molecules and due to the aggregation that occurs between the ZnO NPs. Therefore, it is often necessary to coat these NPs with shells to make them more stable. [33]

1.4.1 Doped ZnO Nanoparticles

For being a wide band gap semiconductor (3.37 eV at room temperature ~368 nm), ZnO requires photons with a wavelength on the UV region to exhibit fluorescence. However, UV light is unsuitable for bioimaging applications since it has reduced penetration depth on tissues and can be harmful to cells, tissues, and live animals. For this reason, most of the conventional fluorescence imaging instruments only have excitation wavelengths of 405 nm or longer. To overcome this issue, several techniques can be used, such as the encapsulation of dyes like FITC on the NPs, coating the NPs with polymers, and by doping elements into the ZnO NPs, to narrow their band gap, being the interest in using doped ZnO nanomaterials for nanomedicine quite recent. So, several different elements have been tested, from which rare earth elements were reported to possess significantly enhanced luminescence, unlike transition metal elements. [21], [29], [30], [34], [35]

ZnO crystallizes in zinc blende (cubic), wurtzite (hexagonal), or rocksalt (cubic) structures. For this reason, ZnO is suitable to be used as a host lattice for lanthanides. However, incorporating ions from these elements into the ZnO lattice remains challenging due to the large difference between their ionic size and charge compared to Zn^{2+}. One of these elements is europium, which can be introduced into the hexagonal zinc oxide matrix by numerous different methods. The improvement in the luminescence on Eu-dopped NPs occurs thanks to the creation of new levels/luminescence centers. These centers lead to the creation of new transitions for the electrons (as can be seen in Figure 1.2), especially when in the presence of other energy trap centers. In this way, it is expected that Eu doped ZnO NPs present higher excitation when using longer wavelengths to excite the electrons and also to present emissions of longer wavelengths. [36]–[40]

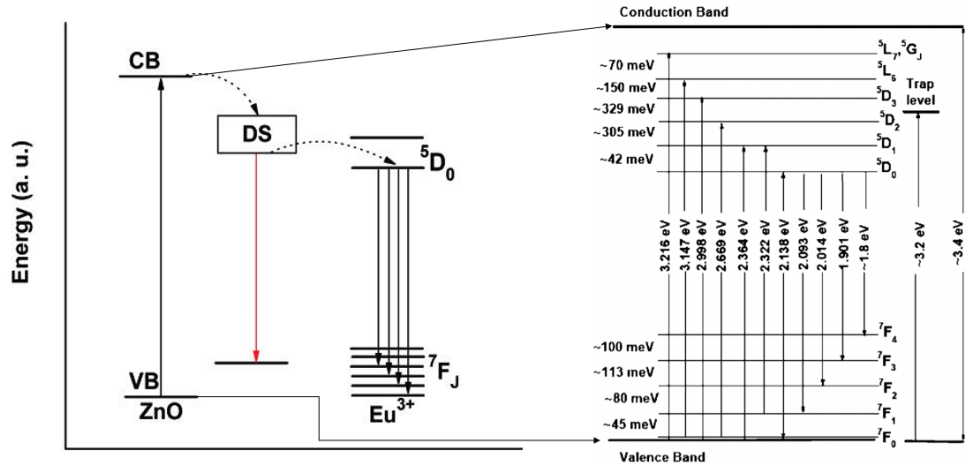

Figure 1.2 - Schematic illustration showing the possible mechanism of energy transfer from ZnO host to Eu^{3+}. (VB represents the valence band, CB represents the conduction band, and DS represents the defect states), and simplified energy diagram of Eu^{3+} in ZnO samples. Adapted from [37] and [36].

In addition to the improvement on optical properties that europium can confer to ZnO NPs, which lead to these NPs to be of interest for bioimaging, photocatalysis and optoelectronic devices, Eu-dopped ZnO NPs have also demonstrated to be a potential tool in cancer radiation therapy by enhancing the X-rays absorption of ZnO nanoparticles and in this way, the properties of these NPs have been of interest in multiple areas. [38], [41]–[43]

However, when using Eu-doped ZnO NPs it is also important to study how the doping of these by europium may affect other properties like their toxicity. In this way, even though on some studies the use of europium in ZnO synthesis being found to not have significant influence on their toxicity further work should be done.[44]

2. Materials and Methods

2.1 Synthesis

ZnO nanoparticles were produced through co-precipitation/microwave-assisted solvothermal methods, using sodium hydroxide (NaOH, ≥98%, labkem, CAS: 1310-73-2) as a precipitation precursor, zinc acetate dihydrate ($Zn(OOCCH_3)_2 \cdot 2H_2O$, ≥98%, Alfa Aesar, CAS: 5970-45-6) and europium (III) nitrate pentahydrate ($Eu(NO_3)_3 \cdot 5H_2O$, 99.5%, Sigma-Aldrich, CAS: 63026-01-7)) as zinc and europium sources and methanol (CH_4O, ≥99.8%, Honeywell, CAS: 67-56-1) and deionized water as solvents. All chemicals were used without further purification.

Zinc acetate was stirred, until complete dissolution, in 33.3 ml of methanol at a concentration of 0.1 M. Several of these solutions were prepared and to each solution, different amounts of europium nitrate were added while stirring to produce doped NPs, with the concentrations of 0, 2, 5 or 10 % mol. Subsequently, 16.7 ml of a stirred solution of NaOH, in deionized water (or methanol), with a concentration ranging from 0.1 M to 0.9 M, were prepared (being most syntheses prepared with 0.3 M) and added to the previous solution while stirring.

To simplify the identification of the most used ZnO NPs samples, to each of them was attributed a letter as shown in Table 2.1 below, being also visible their different syntheses parameters.

Table 2.1 – Letters attributed to the ZnO NPs and their preparation conditions (sample K used europium oxide instead of europium nitrate as Eu^{3+} ions source).

Sample	Letter	%Eu	Annealing	Microwave conditions	Concentration of NaOH used
0% mol Eu.	**A**	0	-	90 ºC 5 min.	0.3 M
2% mol Eu.	**B**	2	-	90 ºC 5 min.	0.3 M
5% mol Eu.	**C**	5	-	90 ºC 5 min.	0.3 M
10% mol Eu.	**D**	10	-	90 ºC 5 min.	0.3 M
700 °C pa 0% mol Eu.	**E**	0	**700 ºC**	90 ºC 5 min.	0.3 M
700 °C a 5% mol Eu.	**F**	5	**700 ºC**	90 ºC 5 min.	0.3 M
700 °C pa 10% mol Eu.	**G**	10	**700 ºC**	90 ºC 5 min.	0.3 M
10% mol Eu. Thigh	**H**	10	-	**130ºC 10 min.**	0.3 M
0.5 mol NaOH RT	**I**	0	-	**-**	**0.5 M**
0.6 molNaOH RT 4% mol.Eu.	**J**	4	-	**-**	**0.6 M**
2% mol. EuO	**K**	2	-	90 ºC 5 min.	0.3 M
Synthesis 6	**L**	0	On this synthesis 7.5 mmol of zinc acetate was put in 75 mL of a mixed solutions of anhydrous ethanol and ethylene glycol, with a volume ratio of 50:25 ml and heated on microwave. As can be seen on annexes.		

After a few minutes under stirring, 25 ml of most of the prepared solutions/suspensions were transferred into a sealed vessel (since the maximum capacity of the vessel was of 25 ml), placed in the microwave synthesizer (CEM Discover SP) and heated until 90 ºC for 5 min. under autogenous pressure with a maximum power of 100 W. Other temperatures and synthesis times were also tested, being other samples either heated to 140 ºC for 10 min. (T_{high}) or not heated, with a reaction time of 5 min.

After synthesis, all produced nanoparticles were centrifuge (HIGH-SPEED Neya 16) at 4000 rpm for 5 min, washed with water and 2-propanol (IPA) and were dried in air at room temperature (RT).

After being dried, some of the produced powders were annealed on the Zabertherm Furnace on-air at 400 ºC and later annealed or reannealed at 700 ºC for 2h.

This synthesis was adapted from previous studies. [35], [42]

A schematic of this synthesis may me observed on Annex Figure A. 1.

In addition to this synthesis, several others were tested. However, these did not seem to provide any additional advantages at the time of selection. [21], [22], [38], [45]–[49]

2.2 Characterization

Scanning electron microscopy (SEM) was performed on Auriga SEM-FIB, Zeiss for morphologic characterization of the ZnO nanoparticles.

Energy Dispersive X-ray Spectroscopy (EDXS) was also performed on the same equipment as SEM to make elemental analysis of the sample.

X-ray diffraction (XRD) was performed on XPert PRO, PANalytical, to study the crystallography of the samples. The X-ray source was Cu Kα, λ =1.54 Å at 45 kV and 40 mA from 2θ = 10 to 90º, at a scanning step of 0.03º and was analyzed using the software "*highscore"*.

Ultraviolet-visible (UV-Vis) spectrophotometry was performed on Perkin Elmer Lambda 950 with a 2 nm step, from λ = 250 nm to λ = 600 nm and with a resolution ≤ 0.05 nm, to obtain the reflection spectra of the produced nanoparticles.

Fluorescence spectroscopy was performed on the Luminescence Spectrometer - Perkin Elmer LS55. Several excitation wavelengths have been used, ranging from 255 to 505 nm at a velocity of 250 nm/min between the wavelengths of 350, 430, or 515 to 700 nm, with low gain and excitation and emission slits at an aperture of 10. The emissions at the wavelengths of 445 and 600 nm were also tested. The used wavelengths were chosen taking into account the wavelengths used in confocal microscopy and in order to be possible to compare the results obtained with those of other articles.

Some of the synthetized samples were also analysed at the University of Aveiro's physics department by steady-state macro-photoluminescence (PL) spectroscopies at RT. For the PL analysis, two different systems and excitation sources were employed. Firstly, the samples were assessed in a Fluorolog-3 Horiba Scientific set-up with a double additive grating Gemini 180 monochromator (1200 gr/mm and 2×180 mm) in the excitation and a triple grating iHR550 spectrometer in the emission (1200 gr/mm and 550 mm), using a 450 W Xe lamp as the excitation source. The same equipment was also used for photoluminescence excitation (PLE) measurements. The PLE was acquired by setting the monochromator on the maxima of the optically active defects and the excitation was scanned to higher energies. Additionally, the samples were excited with the 325 nm line of a He-Cd laser (power density $I_0 < 0.6$ W/cm^2). The luminescence radiation was dispersed by a SPEX 1704 monochromator (1 m, 1200 gr/mm) and detected with a cooled Hamamatsu R928 photomultiplier.

All the above techniques used powdered samples. With the exception of one test on fluorescence spectroscopy that will be later described.

Dynamic Light Scattering (DLS) was performed on the equipment AvidNano W130i as an additional method to determine the nanoparticle size, to study their aggregation velocity and the effect that the use of ultrasounds had on this aggregation. For that, a suspension of ZnO nanoparticles with a concentration of 0.4 mg/ml, which had already undergone ultrasound in the previous week, was used and it was exposed to ultrasound for different amounts of time. Before each measurement, the suspension was stirred to attempt that any bigger NPs that may have been deposited were also measured.

Confocal laser scanning microscopy was performed on the confocal microscope Zeiss LSM 700 and was used to observe the increment on fluorescence that the produced nanoparticles confer to different samples and to compare the properties of these NPs with the commercial fluorophore - fluorescein isothiocyanate isomer I ($C_{21}H_{11}NO_5S$, ≥90%, Sigma-Aldrich, CAS: 3326-32-7) properties. Fluorescence images were obtained through the use of lasers with a λ of 405, 488, and 555 nm and the high-pass filters (only longer wavelengths pass) of 420, 490, and 560 nm respectively, a scan time of 15 seconds per scan, a bit depth of 16 Bit and an average of 2 scans. The pinhole was used on maximum aperture, the digital gain was of 1, the master gain was of 400 or 200 and the intensity of the laser varied from 0.2 to 100% of 5 mW, when the 405 nm laser was used, or 10 mW, when the 488 and 555 nm lasers were used.

To test the nanoparticles in biological samples, onion and human cheek squamous epithelial cells were used, and suspensions with the ZnO NPs in water were prepared with a concentration of 2 mg/ml. A solution of FITC on dimethyl sulfoxide ($(CH_3)_2SO$, ≥99.9%, PanReac, CAS: 67-68-5), with a concentration of 1 mg/ml, was also produced. The onion cells were prepared by peeling the protective skin of an onion layer and putting its outer part facing the microscope slide (Annex Figure A. 2, presented in annexes B). A few drops of the prepared solutions were then added to the sample until this was completely covered, being left to dry. The cheek cells were prepared by first gently scraping the inside of a cheek with a toothpick, then a few drops of the prepared solutions were dropped and drained on the toothpick being the toothpick then smeared on the slide. Before using each ZnO NPs suspensions, these were placed into the ultrasounds for 10 to 15 min to avoid the existence of big agglomerates.

3. Results and Discussion

After the synthesis, even without resorting to characterization techniques, it was possible to observe some differences between the ZnO NPs samples produced with different parameters, such as:

The amount of produced NPs, when using methanol as a solvent for the NaOH solution was much lower than the amount obtained when water was used as the solvent (as can be seen in Figure 3.1).

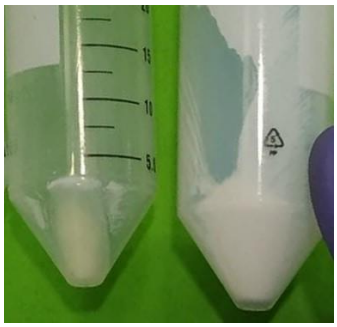

Figure 3.1 – ZnO NPs obtained using NaOH with different solvents: methanol (on the left) and water (on the right)

When using water, 50 ml of the prepared solution resulted in an average of 202 ± 5 mg of ZnO NPs, resulting in a yield of 75 % (calculated by dividing the obtained NPs mass by the maximum mass theoretically obtainable);

While it was possible to verify the precipitation of particles at RT when used a concentration of NaOH ≥ 0.5 M in water, this was not observed for lower concentrations. Lower concentrations seemed to create a gel, only being possible to verify the precipitation of particles after the use of microwave (90 ºC, 5 min);

The use of ultrasounds allowed to disperse the bigger agglomerates formed by the nanoparticles that were visible before the use of these (to better understand the extent to which the nanoparticles de-agglomerated, the DLS technique was used);

After annealing, the powder changed its color from white to yellowish (Annex Figure A. 3);

The fluorescence of the ZnO NPs was visible to the naked eye when using U.V. light as excitation and different synthesis, could emit different colors, emitting synthesis 7 light with green color while most of the other synthesis emitted light with an orange color (Annex Figure A. 4).

3.1 Structural and morphological properties

3.1.1 SEM

Scanning electron microscopy was used to ascertain how the different used synthesis parameters affect the morphology of the ZnO NPs.

Regarding the variations on the microwave synthesis parameters, it was verified that there was practically no interference caused by the synthesis time and temperature on the morphology of the

NPs. This can be seen in Figure 3.2.A and in Figure 3.2.B, where the NPs were in the microwave at 90 and 140 ºC for 5 and 10 minutes, respectively.

It was, nonetheless, observed a significant variation on the NPs size when the concentration of the reagents was changed, as well as when the used solvent was different. The NPs obtained by using higher concentrations of NaOH (Figure 3.2.E) and when using methanol (Figure 3.2.F) instead of water (Figure 3.2.A) as solvent present smaller sizes (33 ± 3, 22 ± 3 and 91 ± 13 nm respectively, measured by using the SEM images with the software *ImageJ*). However, the use of methanol has also demonstrated to be less reproducible since the formation of NPs through this method was not always observed while using similar conditions (Figure 3.2.C).

The doping of NPs with europium has resulted in the appearance of NPs with hexagonal shapes (in addition to the previously obtained NPs) and in a size increase of the NPs, when these were doped with 5 % (Annex Figure A. 5) and 10 % mol. Eu (Figure 3.2.G). On these samples, the NPs with higher dimensions have diameters, ranging from 60 to 220 nm. This increase of the NPs did not happen for the NPs doped with 2% mol. (Figure 3.2.D) and neither on the post-annealed (pa) NPs doped with 10 % mol. Eu, where NPs with bigger dimensions were not observed (Figure 3.2.H).

By using SEM, it was also possible to verify the agglomeration of the NPs (Figure 3.2.I).

As can be observed in (Figure 3.2) most of the formed ZnO NPs were spherical and had a diameter ranging from 20 to 100 nm (depending on the synthesis conditions).

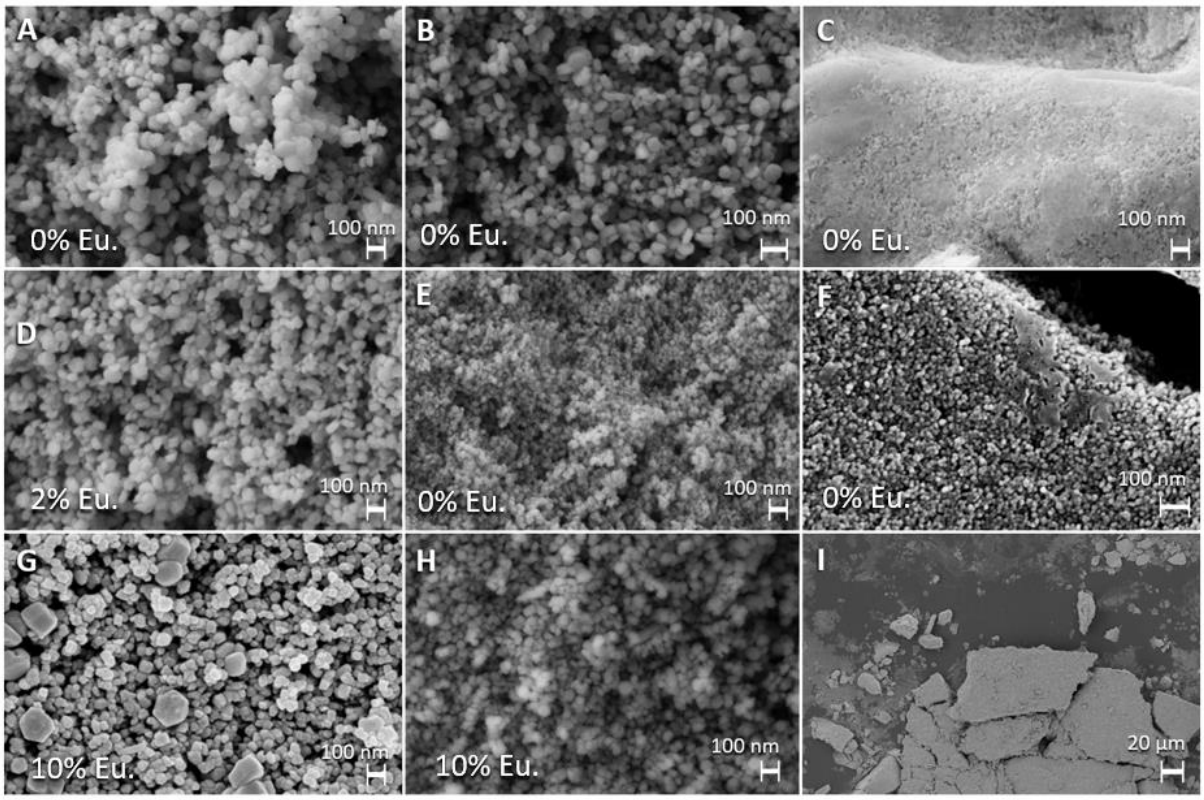

Figure 3.2 - SEM images, of ZnO NPs: A- 0% mol. Eu.; B- 0% mol. Eu $T_{high\ (140\ ºC)}$; C - 0% mol Eu. - methanol; D- 2% mol. Eu.; E- 0.5 M NaOH RT; F- 0% mol. Eu. – methanol; G- 10% mol. Eu.; H- 10% mol. Eu. pa 700 ºC; I- ZnO NPs agglomerates (magnification of 300 ×).

Regarding other syntheses (present on annexes A), the majority also allowed to synthesize identical NPs revealing that there is a wide range of parameters that can be changed to obtain ZnO NPs, which can, in turn, influence the properties of these NPs, however, for seemingly not providing any advantages (like easier synthesis or higher fluorescence) these syntheses were not tested to the same extent. Some of the SEM images obtained for other syntheses can be visualized in Annex Figure A. 5.

Table 3.1 shows the average size of the obtained ZnO NPs produced with different synthesis parameters and europium concentrations.

Table 3.1 – Average ZnO NPs size and standard deviation (obtain through SEM images analyses), letters in parentheses refers to the correspondent SEM images in Figure 3.2.

Sample:	0% mol. Eu. (A)	0% mol. Eu. T_{high} (B)	2% mol. Eu. (D)	0.5 M NaOH RT (E)
Average NPs size (nm):	91 ± 13	98 ± 13	80 ± 12	33 ± 3
Sample:	0% mol. Eu. - methanol (F)	10% mol. Eu. smaller NPs (G)	10% mol. Eu. bigger NPs (G)	10% mol. Eu. Pa 700 °C (H)
Average NPs size (nm):	22 ± 3	54 ± 11	175 ± 27	76 ± 11

As can be seen in Table 3.1, the size of the ZnO NPs can, to a certain limit, be controlled by varying the concentration of NaOH. However, concentrations higher than 0.5 M (0.7 and 0.9 M) did not reveal significant differences in the NPs size. The control of ZnO NPs size by varying the NaOH concentrations has already been observed in other studies being explained that the higher the supersaturation of NaOH, the slower the crystals grow is comparing to the nucleation, which results in smaller crystals. [50]

The changes in morphology observed in ZnO NPs with higher doping concentrations of Eu^{3+} may be attributed to the differences between the ionic radius of Eu^{3+} and Zn^{2+} and on their different electronegativity. [38], [51]

By being spherical and with small dimensions (between 22 and 175 nm), the obtained ZnO NPs seem to have the proper morphologic characteristics to be used in bioimaging. [38]

3.1.2 EDXS

Energy Dispersive X-ray Spectroscopy was used to verify the presence of europium atoms on the obtained ZnO NPs. It was possible to verify a homogeneous distribution of Zn, O, and Eu on the analyzed samples, as well as a much lower amount of europium atoms in comparison with zinc and oxygen, as can be seen in Figure 3.3. Also, since there are no big agglomerations of europium on the samples, it can be assumed that europium was integrated on the ZnO structure or well distributed on its surface.

As seen in Figure 3.3 and Table 3.2, the atomic concentration of europium and oxygen were lower than expected, only appearing to be of 38 or 46 % of oxygen and 0.5 % or 0.1 % of europium on the sample instead of approximately 47.5 and 5%, respectively (as expected). These results may be explained by the fact that EDXS is not a very accurate method to do quantitative analysis of the ele-

ments presented on the sample since this analysis can be affected by several factors, like the overlapping of X-ray emission peaks (in addition to an actual lower concentration of these atoms). [52]

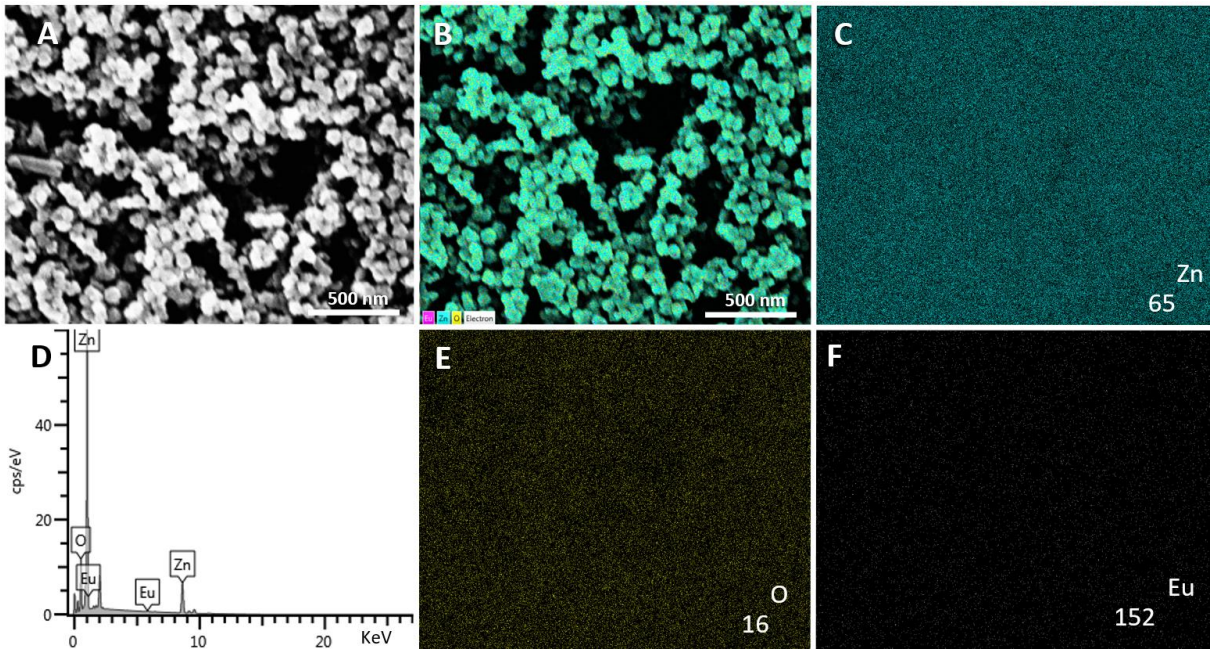

Figure 3.3 – EDXS/SEM images of the 10% mol. Eu. ZnO NPs: A – SEM image of the ZnO NPs; B – Overlay of the SEM image with the elements observed through EDXS; C, E, and F – Zinc, Oxygen, and Europium distribution (respectively) by the EDXS analyses; D – EDXS map sum spectrum of the ZnO NPs.

Table 3.2 - Atomic concentrations obtained by EDXS analyses for the samples 10% mol. Eu. and 10% mol. Eu. Pa700 °C, of oxygen, zinc, and europium.

Element:	**O**	**Zn**	**Eu**
Atomic concentration 10% mol. Eu.:	46.42 %	53.51 %	0.08 %
Atomic concentration 10% mol. Eu. Pa700 °C:	37.97 %	61.57 %	0.46 %

3.1.3 XRD

X-ray diffraction was used to study how the different used parameters have affected the crystallinity properties of the produced ZnO NPs.

The XRD diffractograms of ZnO NPs produced with different concentrations of Eu are presented in Figure 3.4, and it is possible to verify that all the samples present the characteristic peaks of ZnO wurtzite structures, which corresponds to the first three peaks to the family of planes of {1 0 0}, {0 0 2} and {1 0 1} respectively, and that present high crystallinity with no signs of impurities. In addition, the XRD results were used to calculate the grain size, look for the presence of europium on the ZnO crystallite structure, and to see the effects of annealing on the ZnO NPs crystalline structure.

Through the XRD diffractograms, the success of the Eu-doping can be analyzed by looking at the position of the peaks and the cell volume since the ionic radius of Zn^{2+} (0.074 nm) is smaller than the radius of Eu^{3+} ions (0.095 nm). This radius difference leads to the expansion of the lattice parame-

ters for Eu-doped ZnO resulting in a higher cell volume and a shift on 2θ towards the left on the ZnO (0 0 2) peak of the crystals when there is the integration of the Eu^{3+} ions, which may be observed through XRD. [53], [54]

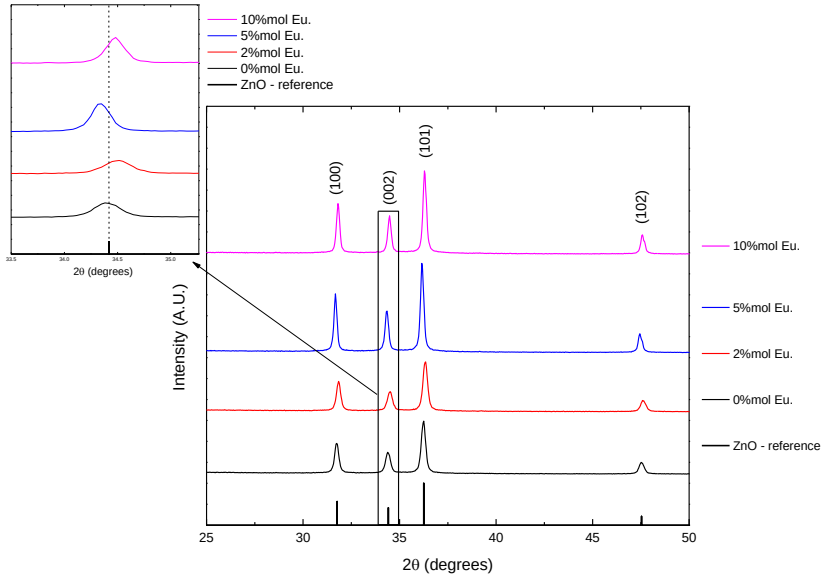

Figure 3.4 - DRX diffractograms of the ZnO NPs doped with 0, 2, 5 and 10 % mol. Eu. and ZnO peaks reference (calculated from *ICSD using POWD-12++*, (1997)).

Moreover, peaks associated with the use of europium, such as europium hydroxide or europium oxide (at 2θ = 29.4° [55]) are not present, which indicates that new form of Eu crystalline structures are not present and that Eu atoms possible were incorporated into the ZnO crystalline structures. This Eu incorporation may happen, either by the substitution of Eu with Zn ions or by the substitution of europium near a zinc vacancy or near an oxygen interstitial [56].

The crystallinity and crystallite sizes of the ZnO NPs can be estimated by the relative intensity of diffraction peaks since lower/broader intensity indicates lower crystallization of the ZnO NPs [57]. Narrower peaks indicate larger crystalline size since larger crystals have crystal planes more align, resulting in higher constructive interference of the X-ray reflected by crystal planes and thus sharper peaks [58]. The crystallite sizes were calculated by using Scherrer's equation (Equation 1) [59], where D is the crystallite sizes, k is the correlation factor (0.89), λ is the used X-ray wavelength (1.5418 Å), β is the full width at half-maximum (FWHM) of the ZnO (101) peak for being the preferred orientation since it is the most prominent diffraction peak, and θ is Bragg's diffraction angle [51]. The obtained values are presented in Table 3.3.

$$D = \frac{k\lambda}{\beta \cos\theta} \qquad \text{(Equation 1)}$$

As can be seen in Figure 3.4 and Table 3.3, through the observation of the position of the peaks, it is not evident a relationship between their position and the Eu doping concentrations. The differences in the magnitude of doped and un-doped ZnO NPs are also observed between un-doped ZnO NPs and on repeated tests. This might indicate that the Eu^{3+} ions reside on the surface of the ZnO NPs.[60] Regarding the cell volume of the Eu-doped ZnO NPs, even though there was a slight in-

crease in the cell volume of the 10 % mol. Eu-doped ZnO NPs, the observed difference may be too small to draw any conclusions. Since there are no Eu-associated peaks, the structure of the ZnO NPs was not modified by the addition of Eu into the ZnO matrix. One possible explanation for this is that europium has not integrated well into the ZnO structure due to its high atomic size.

As expected, the crystalline size was lower than the NPs sizes, observed through SEM, and was bigger for the Eu doped ZnO NPs, produce at 90 ºC for 5 min. but was not bigger for the Eu doped NPs produced at higher temperatures. Contrary to expectations, the annealed ZnO NPs present a smaller crystallite size than the NPs that were not annealed. This might be due to an unnoticed difference in their syntheses since the annealed ZnO NPs are not the same as the ZnO NPs measured after annealing, but rather other synthesized ZnO NPs after annealing.

Table 3.3 – Peak characteristics of the tested ZnO NPs and their cell volume, structure, and crystallite size (obtained with Scherrer's equation).

Sample	(002) peak (2θ degrees)	(101) peak (2θ degrees)	FWHM of (101) peak (2θ degrees)	Crystallite size (nm)	Cell volume (10^6 pm^3)	Structure
ZnO 0% mol Eu.	34.372	36.206	0.232	35.653	47.63	Hexagonal
ZnO 2% mol Eu.	34.471	36.300	0.243	34.049	47.63	Hexagonal
ZnO 5% mol Eu.	34.312	36.140	0.156	53.013	47.63	Hexagonal
ZnO 10% mol Eu.	34.449	36.273	0.167	49.540	47.76	Hexagonal
700 ºC annealed ZnO 0% mol. Eu.	34.512	36.349	0.306	27.042	47.63	Hexagonal
700 ºC annealed ZnO 5% mol. Eu.	34.425	36.259	0.340	24.332	47.58	Hexagonal
700 ºC annealed ZnO10% mol.Eu.	34.549	36.375	0.298	27.770	47.58	Hexagonal
0.3 M NaOH ZnO - RT	ZnO NPs were not obtained with these conditions					
0.5 M NaOH ZnO - RT	34.426	36.266	0.495	16.713	47.63	Hexagonal
ZnO 10% mol. Eu. T_{high}	34.464	36.285	0.323	25.614	47.58	Hexagonal
0.6 M NaOH ZnO RT 4%mol. Eu.	34.331	36.184	0.439	18.841	47.62	Hexagonal

In figure 3.5 is possible to observe the XRD diffractograms of ZnO NPs produced with different concentrations of NaOH added to the synthesis solution, as well as the 10% Eu dopped ZnO NPs submitted to other conditions. The 0.3M and 0.6M synthesis occur without the use of microwave irradiation, showing that only by using a higher concentration of NaOH was possible to obtain ZnO NPs. It was not verified any significant difference between XRD diffractograms of the Eu. doped ZnO NPs.

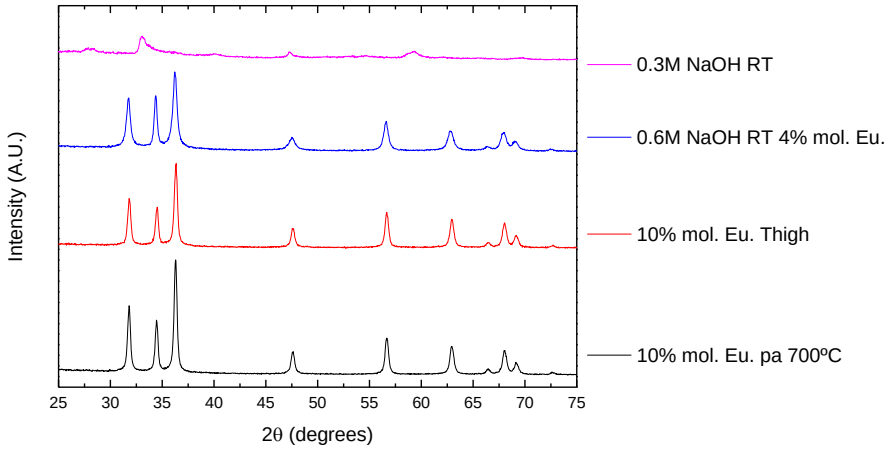

Figure 3.5 – XRD diffractograms of the ZnO NPs of 0.3M NaOH RT, 0.6M NaOH RT 4% mol. Eu, 10% mol. Eu T_{high} and 10% mol. Eu pa 700 ºC.

The XRD diffractograms graph obtained for different syntheses can be observed in Annex Figure A. 6.

3.1.4 DLS

To evaluate the particle size and the aggregation tendency of ZnO NPs, dynamic light scattering (DLS) was used. Also, it was evaluated the use of ultrasounds to desegregate the ZnO NP.

As can be observed in figure 3.6, through the use of DLS, the NPs presented a hydrodynamic diameter, approximately between 80 and 350 nm, which is slightly higher than the values obtained through SEM (between 91 and 175 nm).

It was also possible to verify a slightly bigger size of the Eu. doped ZnO NPs (188 ± 79 compared to 137 ± 65 nm). It should be stressed that this technique does not actually measure the diameter of the NPs but the hydrodynamic diameter of any particle on the solution (being these particles an aggregation of NPs or not). In this way the obtained dimensions are higher than the actual size of the NPs since, the hydrodynamic diameter is the calculated diameter for a hypothetical hard sphere that diffuses with the same speed as the particle being measured. [61]

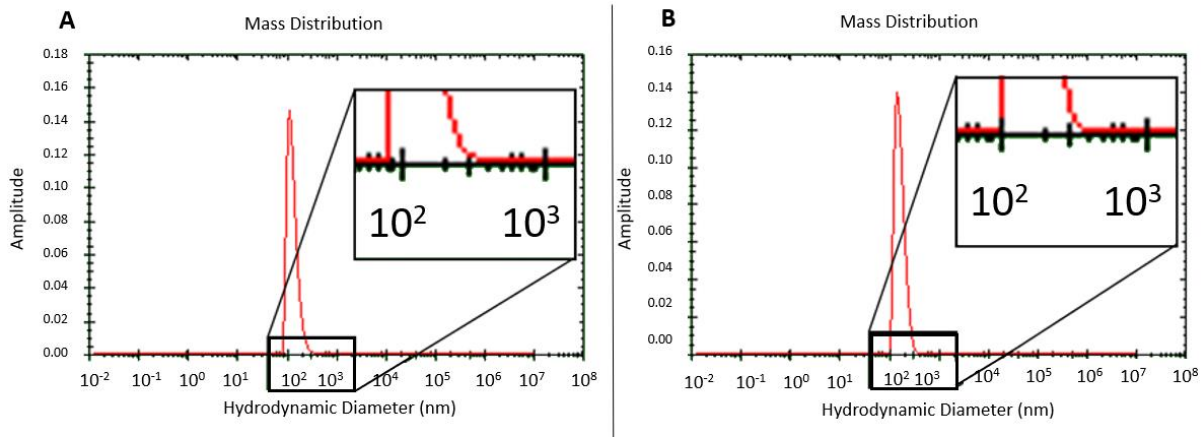

Figure 3.6 – DLS mass distribution graph of NPs doped with 0 (A) or 10% Eu. (B) after the use of ultrasounds for 15 min.

Regarding the ultrasound effects, as expected, the size of the particles decreased with the time they were exposed to ultrasounds, especially in the first 2 minutes. In contrast, particle size increase with time after being removed from ultrasounds (as can be seen in Table 3.4). This decrease and increase happen due to the desegregation and aggregation of NPs. However, these results must be analyzed with some skepticism since the standard deviation is very high (above 100 nm in some cases) and even though most results were constant, considerable variations were observed for some tests.

Regarding the measurements after the use of ultrasounds, before each measurement, the suspension was stirred to disperse any bigger particles that may have been deposited. By not doing so, the hydrodynamic diameter would decrease as the larger particles would be deposited, being only the smaller NPs (or aggregates of NPs) in suspension measured. It can also be observed that the aggregation of the NPs does not appear to be very fast (Table 3.4).

Table 3.4 - DLS analyses on the aggregation/desegregation, over time, of the ZnO NPs with the use of ultrasounds.

Time on ultrasound	**0 min.**	**1 min.**	**2 min.**	**4 min.**	**15 min.**
0% Eu.	1852 nm	354 nm	193 nm	200 nm	191 nm
10% Eu.	5584 nm	636 nm	310 nm	286 nm	237 nm
Time after ultrasound	**2 min.**	**15 min.**	**30 min.**	**40 min.**	**50 min.**
0% Eu.	185 nm	200 nm	206 nm	211 nm	212 nm

3.2 Optical properties

3.2.1 UV-Vis spectrophotometry

UV-Vis spectrophotometry was used to study how the different synthesis parameters affected the absorbance/reflectance of the ZnO NPs samples and their band gap.

In figure 3.7 is possible to observe the reflectance spectra of ZnO NPs produced with different concentrations of Eu. before and after annealing.

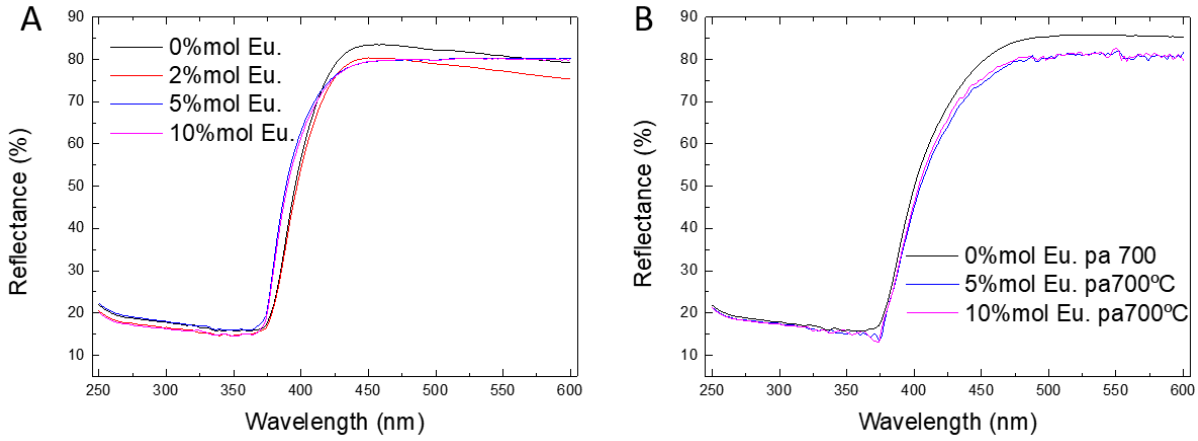

Figure 3.7 - Reflectance spectra of the ZnO NPs doped with different concentrations of Eu (A) before annealing and (B) after annealing.

As can be seen in Figure 3.7, the addition of europium and the annealing treatment of Eu doped ZnO NPs seem to alter the reflectance spectra, having un-annealed Eu. doped ZnO NPs a slightly lower ability to absorb light of the wavelengths between 375 and 410 nm than the undoped and un-annealed ZnO NPs.

Through the reflectance spectra, it can also be obtained the ZnO NPs band gap by using the Tauc's plot method. This method assumes that the energy-dependent absorption coefficient (α) can be expressed by the following equation:

$$(\alpha h\nu)^{1/\gamma} = A(h\nu - Eg) \qquad \text{(Equation 2)}$$

Where h is the Planck constant, ν is the photon's frequency, Eg is the band gap energy, and A is an energy independent constant that measures the disorder of the material.[62] The γ factor depends on the nature of the electron transition and is equal to 1/2 or 2 for the direct (as is the case for ZnO) and indirect transition band gaps, respectively. By applying the Kubelka–Munk function (F(R∞), (Equation 3)), the measured reflectance spectra can be transformed to the corresponding absorption spectra, where R∞ represents the reflectance of an infinitely thick specimen. [63]

$$F(R\infty) = \frac{(1 - R\infty)^2}{2R\infty} \qquad \text{(Equation 3)}$$

By using these equations, the graphics in Figure 3.8 were obtained, being possible to obtain the band gap of ZnO NPs by doing a linear regression and calculating the value at which that linear regression intersects the x-axis. The same method was used to determine the band gap of other ZnO NPs present in Table 3.5.

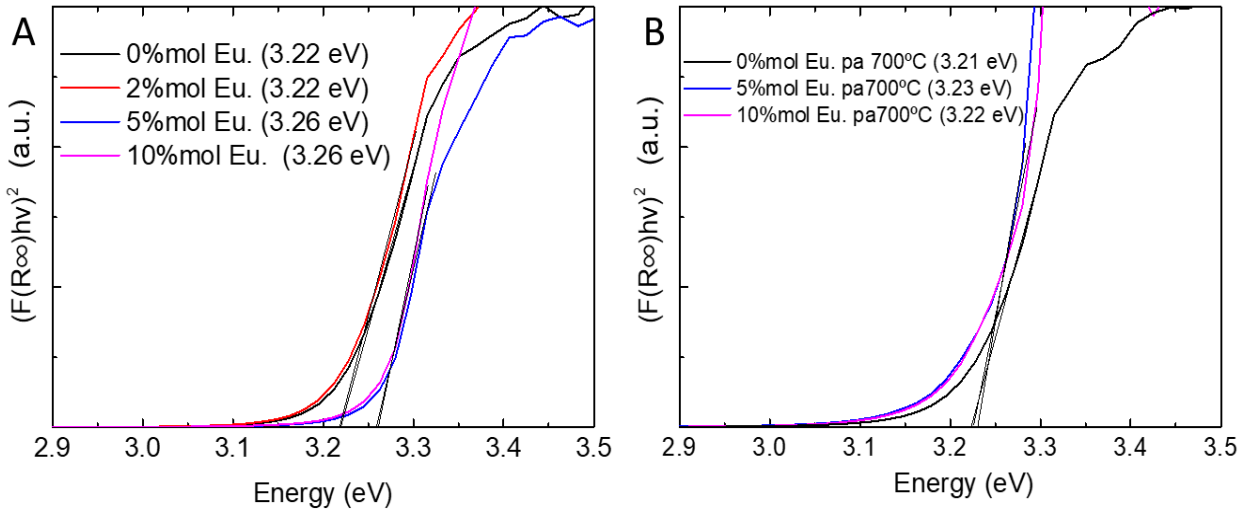

Figure 3.8 - Band gap energy (Eg) determination from the Tauc plot of the ZnO NPs synthesized with different concentrations of Eu (A) before and (B) after annealing

Table 3.5 – Band gap energy of ZnO NPs produced with different concentrations of Eu, before and after annealing.

ZnO NPs:	**0% mol Eu.**	**2% mol Eu.**	**5% mol Eu.**
Band gap (eV):	3.22	3.22	3.26
ZnO NPs:	**10% mol Eu.**	**700°C pa 0% mol Eu.**	**700°C pa 5% mol Eu.**
Band gap (eV):	3.26	3.21	3.23
ZnO NPs:	**700 °C pa 10% mol Eu.**	**0.5mol NaOH RT**	**10% mol Eu. T_{high}**
Band gap (eV):	3.22	3.21	3.23

As expected through the analyses of the reflectance spectra, the Eu doped NPs (at a concentration of 5 or 10% mol.) presented slightly higher band gaps than pure ZnO NPs. So, there seems to be some correlation between the band gap and crystalline size (Annex Figure A. 7), having the smaller ZnO NPs (0.5mol NaOH RT) one of the smallest band gaps (3.21 eV), as reported in other studies [64], [65]. This correlation was not observed between the band gap and Eu. doping since, for example, the doped samples synthesized at higher temperature did not present an increase in their band gap (and neither on their crystalline size), as can be seen in Annex Figure A. 8.

3.2.2 Fluorescence spectroscopy

Fluoresce spectroscopy was used to study how different excitation wavelengths (255, 325, 380, 393, 400, 405 and 464 nm) and different synthesis parameters affect the fluorescence of the produced ZnO NPs.

Through the use of the Luminescence Spectrometer - Perkin Elmer LS55, it was possible to verify some peaks associated with ZnO when using an excitation wavelength of 255 nm (at 425, 490 and 534 nm), as can be seen in Figure 3.9.B [28]. However, it was not fully clear the appearance of all the peaks and it was difficult to verify well-defined peaks associated with europium doping (Figure 3.9.A). It was only possible to identify the europium related peaks at 595 and 618 nm for a few samples when using an excitation of 405 nm, not being possible to identify the peaks at 577 nm, 648 nm and 697 nm for any of the samples [36]. Additionally, it was not possible the comparison between the samples intensities, due to a great dependence of the sample intensity with the distribution of the powder when preparing the samples for measurement (Annex Figure A. 9). The only sample of ZnO NPs that revealed a higher difference in the intensity was the one in which it was tried to encapsulate ZnO with silica (present on Annex A - Seventh method). This synthesis enabled a much higher intensity for excitations of shorter wavelengths (U.V. region) (Annex Figure A. 10), however this was not observed for longer wavelengths.

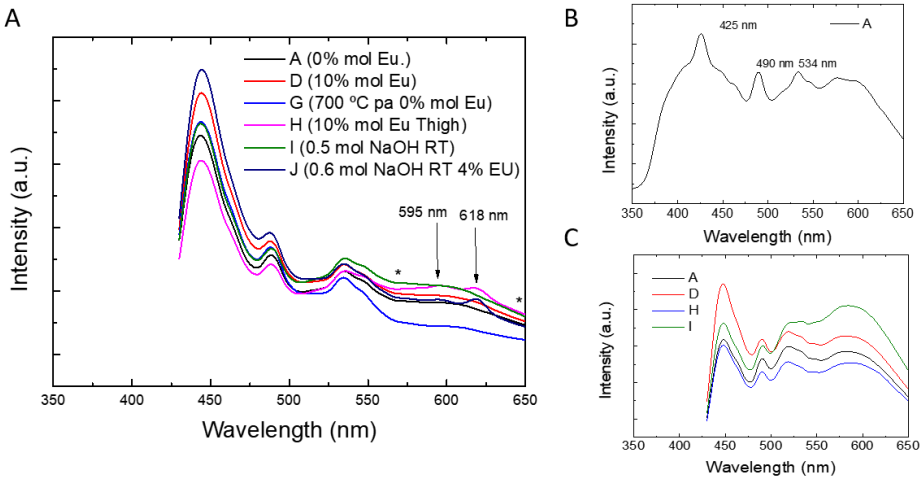

Figure 3.9 - Room temperature photoluminescence spectra of ZnO NPs and Eu doped ZnO NPs synthesized by using different parameters, using excitation wavelengths of 405 nm (A), 255 nm (B), and 380 nm (C). Asterisks on (A) mark other peaks related to Eu doping.

As can be seen in Figure 3.9.A, ZnO NPs seem to present high fluorescence for an excitation wavelength of 405 nm and thus, may be used on confocal microscopy.

To better understand the dependence of ZnO NPs fluorescence with its synthesis parameters, steady-state macro-PL spectroscopies analysis was also performed on some of the ZnO NPs that previously have shown better results. The results are shown in figure 3.10.

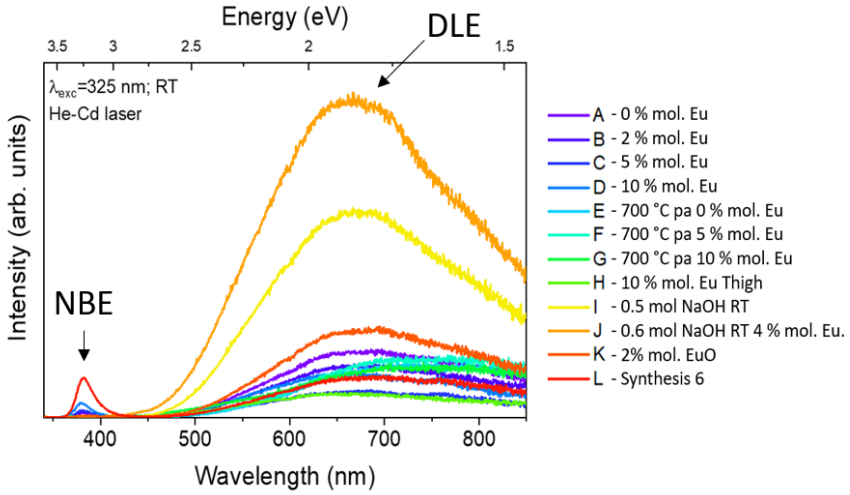

Figure 3.10 - Room temperature photoluminescence spectra with an excitation wavelength of 325 nm of ZnO and Eu doped ZnO NPs synthesized using different parameters.

As can be observed in Figure 3.10, after being excited with the 325 nm laser (3.8 eV), most of the ZnO NPs present near band edge emission (NBE), and a much stronger deep-level emission (DLE) peaked in the orange/red spectral region, characteristic of ZnO luminescence [66]. This difference in intensity was mainly observed for the ZnO NPs I, J, H, and K, being the DLE much stronger on I and J than on other samples, while the H and K samples reveal a NBE strongly quenched or evenly absent.

The much stronger DLE of the samples I and J may be explained by their smaller size and crystallite size (16.7 nm and 18.8 nm, respectively) since DLE is caused by defects in the ZnO crystalline

structure. Thus, more intense DLE indicates a strongly defected structure of crystals. The much higher intensity observed on sample J may also indicate that, as observed in other studies, the high surface to volume ratio of the NPs strongly influences the intensity of europium luminescence, suggesting that Eu^{3+} ions may predominantly be grouped on the surface of the ZnO crystals. [38]

Contrary to these samples, sample L (synthesized by a different method) showed a higher ratio between tNBE/DLE intensities, revealing how different synthesis influence the ZnO NPs properties.

Moreover, it is also possible to observe a red-shift for the samples E, F and G (which were annealed at 700 ºC), having their peak on the wavelength of 740 nm, instead of 680 nm (as was observed for the un-annealed samples). This red shift was also observed in other studies, however contrary to some of these studies, the red-shift cannot be attributed to the increase in the crystallite size of the NPs since annealed samples did not present a larger crystallite size [67], [68]. So, the red-shift may be attributed to the high annealing temperature leading to Zn-related defects and/or oxygen vacancies since annealing was performed in air, as can be observed on the EDXS results. However, excess of oxygen has also been attributed to this shift [66].

On the annealed samples, a reduction of the NBE intensity was also visible.

It should be highlighted that these results may not be directly used to evaluate the fluorescence that the different ZnO NPs would present in fluorescence microscopy since the reduced wavelength and high intensity used on this analysis are not usually used on fluoresce microscopy.

Regarding the PL and PLE spectra analyses in Figure 3.11 and Figure 3.12, these may better reflect the optical properties of the NPs when used in confocal microscopy because, in addition to also analysing longer wavelengths, the used excitation intensity was much lower than the used intensity on previous analyses (as it is usually used on confocal microscopy, and especially in biological samples). By using smaller excitation intensity, it was noted that the DLE presented a blue-shift for all the samples when using a 325 nm beam and thus, the DLE is sensitive to the excitation intensity. More specifically, when using a lower beam intensity, the DLE presented an emission peak at 560 nm instead of 680 nm.

Concerning the effects of Eu doping, it is possible to observe, in Figure 3.11.A, that the Eu doped samples (B, C, and D) do not show any clear peaks associated with the intraionic transition of Eu^{3+}, being only possible to observe a small peak at 613 nm on the samples C and D (doped with 5 and 10% Eu.). This peak corresponds to the $^5D_0 \rightarrow {}^7F_2$ transition of the Eu^{3+} [36]. The 613 nm peak is more evident on the annealed samples F and G, as can be seen in Figure 3.11.B, indicating that annealing may favour the ion optical activation (however, it is important to notice that the annealed samples are not the samples A, C, and D after annealing).

Even though there are no clear peaks on sample B, C, and D, the influence of europium is clearly visible, having the higher Eu doped NPs, higher emission on shorter wavelength values for the 400 nm excitation, and higher emission for longer wavelengths values on the PLE spectra of the 565 nm emission. In this way, it is possible the use of longer wavelengths for the fluorescence of the Eu doped ZnO NPs. The increase in intensity on the PLE spectra is also observed on the doped annealed samples.

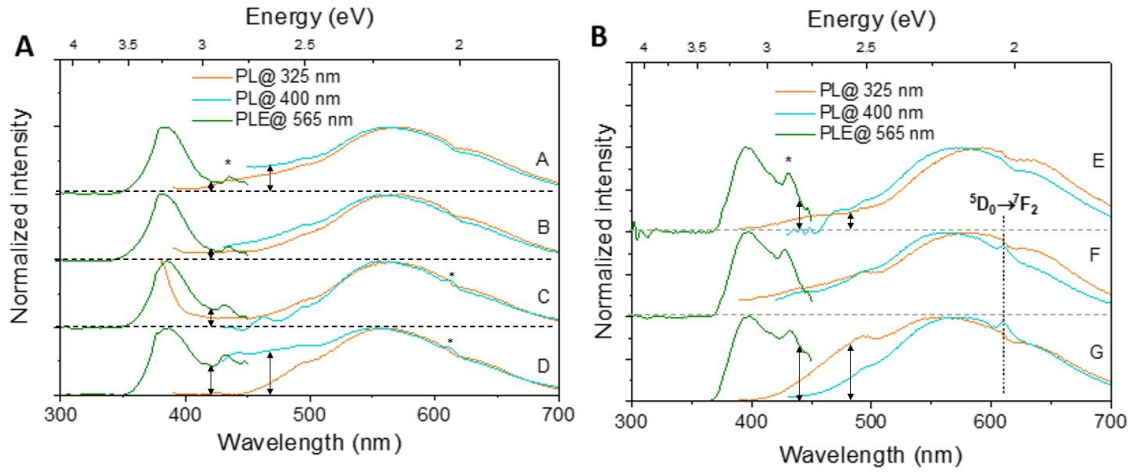

Figure 3.11 - Room temperature photoluminescence and photoluminescence excitation spectra of undoped and Eu doped ZnO samples (the asterisk on the 440 nm peak represents artefacts and the asterisk at the 613 nm highlights the small peak that is visible at that wavelength). A- Un-annealed samples B- Annealed samples.

As can be seen in Figure 3.12.A the analyses performed on samples H to L revealed that with the variation of a few parameters, it is possible to obtain an intraionic transition of Eu^{3+} (on the Eu doped samples: H, J, and K). This effect is especially visible on sample H, which is similar to sample D but was synthesized by using higher time and temperature on its synthesis. In sample H, in addition to being visible the previously observed peak at 613 nm ($^5D_0 \rightarrow {}^7F_2$), the peaks (and their correspondent transition) at 577 nm ($^5D_0 \rightarrow {}^7F_0$), 591 nm ($^5D_0 \rightarrow {}^7F_1$), 648 nm ($^5D_0 \rightarrow {}^7F_3$) and 697 nm ($^5D_0 \rightarrow {}^7F_4$), were also observed, remaining the 613 nm peak the most intense [36].

One other aspect that can be studied by observing the peaks is the crystal symmetry of the samples, making it possible to characterize the incorporation of the Eu ions in the ZnO lattice. This happens since, while the transition $^5D_0 \rightarrow {}^7F_2$ (614 nm) of Eu^{3+} is very sensitive to the local crystal symmetry and its transition probability is zero if the Eu^{3+} ions are embedded in a centro-symmetric environment (presenting lower intensity on the PL spectra), this does not happen to the $^5D_0 \rightarrow {}^7F_1$ (590 nm) transition which intensity does not variate with the local crystal symmetry. In this way, the smaller the intensity ratio between the $^5D_0 \rightarrow {}^7F_2$ /$^5D_0 \rightarrow {}^7F_1$ transitions is, the lower is the distortion of the symmetry around the Eu^{3+} ions in the ZnO lattice. By observing the PL spectra of the samples is visible that the $^5D_0 \rightarrow {}^7F_2$ transition has higher intensity indicating that the Eu^{3+} ions may not have substituted the Zn^{2+} and were placed on lower symmetry sites, and thus may be located on the surface of the nanocrystals. This is also suggested by the appearance of the $^5D_0 \rightarrow {}^7F_0$ peak (on sample H). [36], [38], [39]

Even though samples H and J have shown an increase, in intensity, of the peaks associated with Eu^{3+} ions, these samples did not show as much, the other previously observed optical changes, such as the increase in intensity on the shorter wavelength values, for the 400 nm excitation. In addition to this, only sample H shows an increase in longer wavelength values for the 565 nm emission. In this way, these samples may not be the best FPs for confocal microscopy when compared with sample D.

The increase in the intensity on the shorter wavelength values for the 400 nm excitation and on the longer wavelength values for the 565 nm emission was only observed when Eu was used, with the exception of sample L, which was synthesized by another method revealing that the synthesis method

is as important to analyze as the doping of the samples. Yet, it was not well determined what caused this increase in the optical properties of sample L. One hypothesis might be related to its small crystalline size since it presents the smallest calculated crystalline size of 13 nm and thus has a larger surface area (to volume). This may lead to the presence of more oxygen vacancy defects and thus higher visible emission, but this was not observed when using a wavelength of 325 nm. In this way more studies should be done in order to better understand to what extent the different synthesis and different doping concentrations of europium may influence the ZnO NPs fluorescence. [45]

To better examine the Eu related peaks present on the samples, PLE with the wavelengths of 590 nm ($^5D_0 \rightarrow {}^7F_1$) and 612 nm ($^5D_0 \rightarrow {}^7F_2$) was made, as well as PL with the wavelengths of the higher peaks obtained from the PLE spectra (393 nm and 464 nm). These tests were made on samples H and J, for being the ones with the highest intensity of Eu^{3+} emission peaks (Figure 3.12.B).

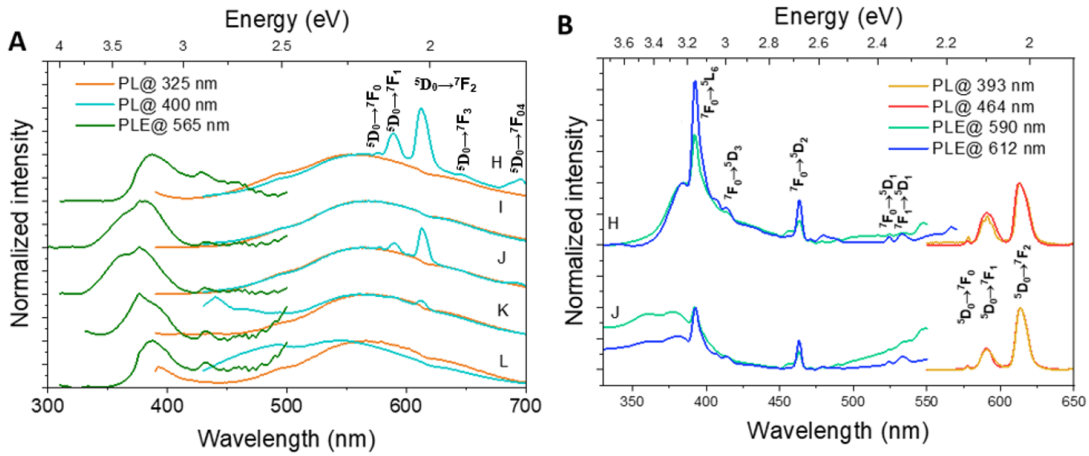

Figure 3.12 - Room temperature photoluminescence and photoluminescence excitation spectra of undoped and Eu doped ZnO samples.

Through the PLE analyses was possible to verify the existence of five peaks related to Eu ions excitation, associated with the transitions393 nm ($^7F_0 \rightarrow {}^5L_6$), 414 nm ($^7F_0 \rightarrow {}^5D_3$), 463 nm ($^7F_0 \rightarrow {}^5D_2$), 524 nm ($^7F_0 \rightarrow {}^5D_1$) and 534 nm ($^7F_1 \rightarrow {}^5D_1$).

So, it was possible to verify the presence of Eu on the samples and the effect on the optical properties of the ZnO NPs, especially when excited with the wavelength of 400 nm (closer to the one used on confocal microscopy).

One other studied aspect through fluorescence spectroscopy was the fluorescence stability of the ZnO NPs in water since, has been reported that the surface luminescent centers of ZnO NPs can be rapidly destroyed by water molecules due to the destruction of surface defects of ZnO, leading to fluorescence quenching [21], [33]. In addition to this, the aggregation/precipitation of the ZnO NPs was also investigated.

To study this effect, suspensions of 0.4 mg/ml of ZnO NPs on water and ethanol were produced and placed in the ultrasounds for about 10 minutes, being measured the fluorescence immediately after the preparation, after 30 min. and after one week, by using an excitation radiation of 405 nm. The results after one week were also measured after the suspension was resubmitted to ultrasounds.

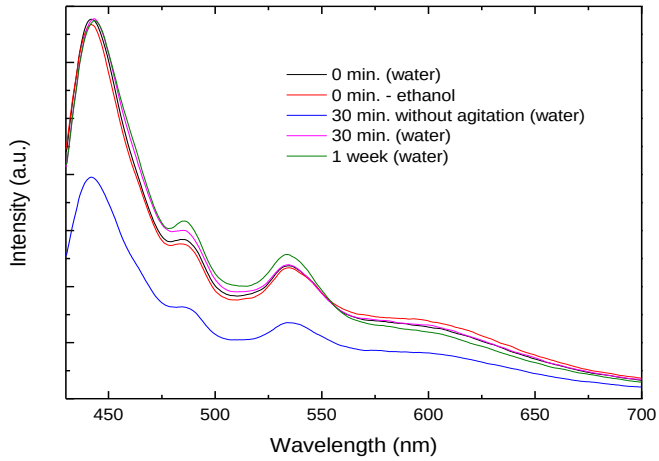

Figure 3.13 – Variation of Room temperature photoluminescence spectra intensity (excitation wavelength of 405nm) of ZnO samples on a suspension of either ethanol or water for different amounts of time.

As can be observed in Figure 3.13, it was not visible any decrease of fluorescence when using water instead of ethanol, as well as it was not observed a reduction in fluorescence on the NPs when using water after one week (just as it was not seen after 30 min.). In this way, ZnO NPs fluorescence does not seem to be quenched by water and thus its fluorescence has a high stability in water. It can also be observed the substantial decrease in the fluorescence 30 min. after the first measurement due to the rapid precipitation of the ZnO NPs on the sample that was not stirred.

3.2.3 Confocal laser scanning microscopy

In order to study the optical properties of fluorescence of the ZnO NPs in a medium more similar to the final objective, the use of nanoparticles in biological samples of onion cells and human cheek squamous epithelial cells was tested. Wavelengths of 405, 488, and 555 nm (and their respective filters) were used and the images obtained were mainly colored in gray, green and red, according to the used wavelength (correspondingly).

It should be noted that the nanoparticles were not targeted to any specific element of the samples, and thus, their accumulation on the sample was spontaneous.

In addition, to studying the behavior/properties of the ZnO NPs on the cells, these NPs were also compared with the commercial fluorophore FITC on several aspects.

Initially, to verify if it was possible to observe fluorescence directly from the samples, the samples 0%, 10%, and 10% T_{high} mol. Eu. (A, D and H), were placed on a microscope slide and directly observed on the confocal microscope using an excitation wavelength of 405 nm. It was only possible to observe fluorescence on the sample 10% mol. Eu. (sample D), as can be seen in Figure 3.14 (colored in orange for better visualization), and so, this sample was one of the most used on the following experiences.

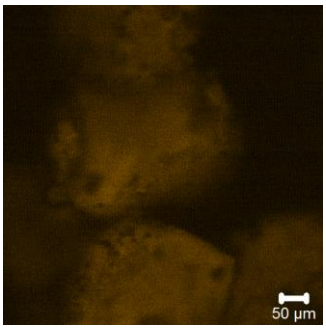

Figure 3.14 –Confocal microscope image of ZnO NPs doped with 10% mol. Eu, using an excitation wavelength of 405 nm.

In this way, as previously noted, europium seems to have increased the fluorescence of the ZnO NPs. However, the samples in which the highest fluorescence was observed were not necessarily the ones that had the presence of the most intense Eu related peaks (like sample H) but the ones in which the increase of shorter wavelength emission for visible wavelength excitation (400 nm) was noticeable (like sample D).

To check the use of ZnO nanoparticles as a potential biolabel for bioimaging applications, its use in onion and cheek cells was tested, being the onion cell the most used. These were the cells chosen for analysis because they are easy to obtain and prepare for observation on the confocal microscope with the ZnO NPs. However, these cells, and in particular onion cells, also showed significant fluorescence/artifacts, especially on the cell wall, as can be seen in Figure 3.15, making it challenging to easily visualize the fluorescence that the ZnO NPs conferred to these cells.

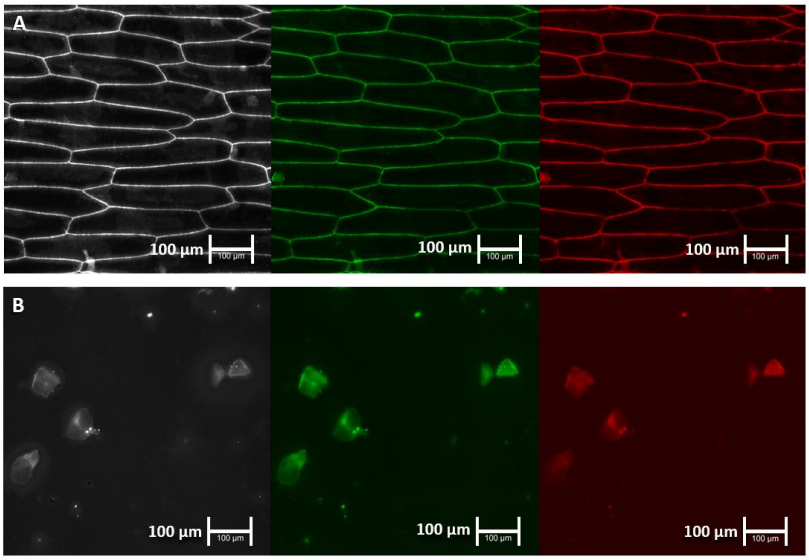

Figure 3.15 – Intrinsic fluorescence of onion (A) and cheek cells (B) when using the excitation wavelengths of 405, 488, and 505 nm (respectively, on the images from the left to the right) on confocal microscopy, using an intensity of 60 % and gain of 400.

To overcome the intrinsic fluorescence/artefacts of these cells, confocal images with the same used parameters were also obtained for cells without the NPs and a comparison between these was made. Since water was used for the NPs suspensions, it was also checked for any additional fluorescence attributed to water (which was not observed). The images of onion cells that allowed a better

contrast between the cell wall and the cell's interior were used as the control since this difference could vary greatly from sample to sample, being, for example, samples with higher-sized cells easier to observe the cell wall.

To study the additional fluorescence conferred by nanoparticles to onion cells, ZnO NPs suspensions, doped with different Eu concentrations, were dropped until the onion cell was covered entirely. The onion cell with ZnO NPs was then left to dry. As can be seen in Figure 3.16, after the addition of the ZnO NPs into the onion cells and using an excitation wavelength of 405 and 488 nm, it is possible to observe a higher fluorescence when comparing with cells without ZnO NPs, being easy to observe a higher contrast between the inside of the onion cell and its walls. This contrast was more evident when using ZnO NPs doped with Eu.

The main reason for the increase of fluorescence on the cell walls and not on the whole cell resides in the fact that it is estimated that the pore size of the cell wall ranges from 5 to 20 nm. Thus, only NPs or NPs aggregates with diameter inferior to the pore diameter of the cell wall can easily pass through and reach the plasma membrane and thus, the NPs were mainly accumulated on the outside, between the cells walls, increasing the luminescence on these places (since all the produced NPs have a diameter superior to 30 nm). [69], [70]

The same behavior was not observed when using an excitation wavelength of 555 nm (as can be seen in Figure 3.16), being only possible to visualize the cell walls of the sample when using high laser intensity. This happens due to the photons of the 555 nm laser possessing smaller energy and thus not having enough energy to excite the electrons and, in this way, create fluorescence.

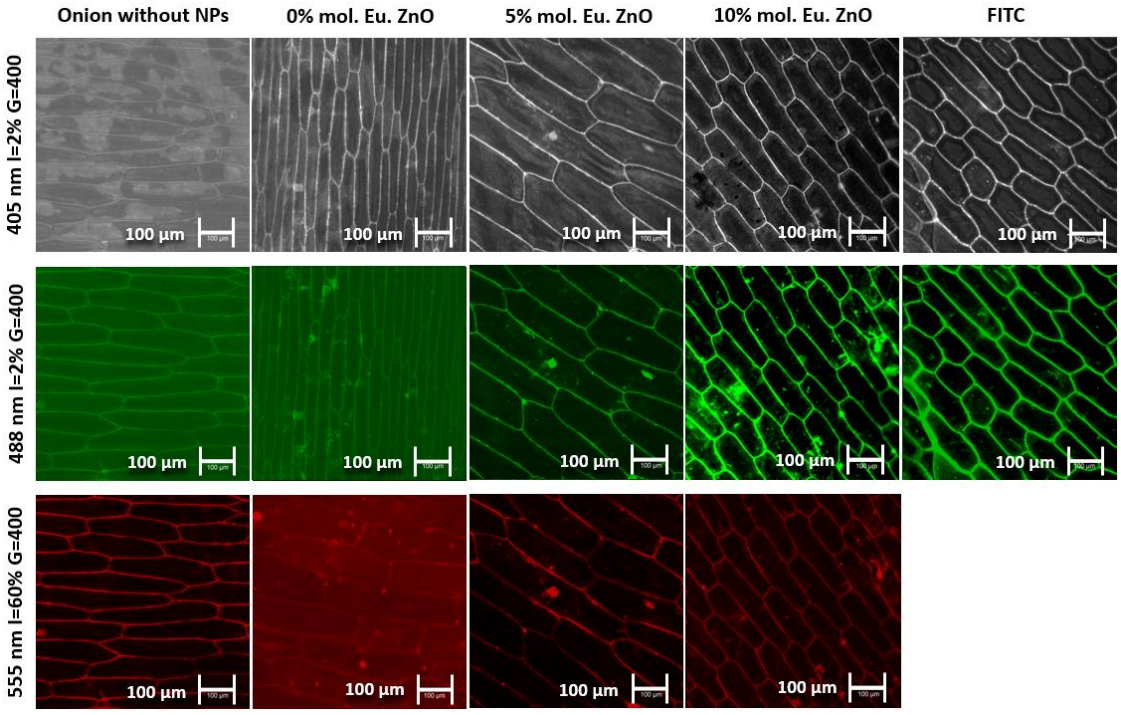

Figure 3.16 – Variation of the fluorescence intensity, when using onion cells, (from the left to the right column) without ZnO NPs and with 0, 5, 10 % mol. Eu ZnO and FITC, when submitted to the different laser excitations wavelengths (top line - wavelength of 405 nm, intensity of 0.1 mW and gain of 400; middle line – wavelength of 488 nm intensity of 0.2 mW and gain of 400; bottom line wavelength of 555 nm, intensity of 6 mW and gain of 400). All the images were obtained by using the same magnification.

Another noted difference was between the fluorescence intensity observed on the cells when using the wavelengths of 405 nm and 488 nm (as can be seen in Annex Figure A. 11). Between these wavelengths, contrary to expectations, the 488 nm laser appears to produce higher fluorescence even when used lower laser intensities than the 405 nm laser. The 405 nm laser was expected to produce higher fluorescence since the photons of the 405 nm laser have higher energy and appeared to produce higher fluorescence on the fluorescence spectroscopy analyses.

When analyzing the sample 10% mol. Eu. ZnO by using the 488 nm laser, it is possible to differentiate the cell wall using only 0.2% (= 0.02 mW) of the laser intensity. However, for the 405 nm laser, it had to be used 1.5% (= 0.075 mW) of the intensity to visualize the same.

This difference may be explained due to the used filters since the 488 nm laser uses high-pass filters at 490 nm and thus, an interval of only the 2 nm higher than the excitation wavelength of 488 nm is filtered out. However, for the 405 nm laser, the filter is located at 420 nm, cutting out the wavelength interval of the 15 nm higher than the excitation wavelength of 405 nm. In this way, less fluorescence is observed for the 405 nm laser when comparing with the 488 nm laser.

In addition to this, the higher fluorescence when using the 488 nm laser was also observed when using onion cells without NPs, once again indicating that the difference in fluorescence when using these two wavelengths may not be thanks to a higher produced fluorescence by the 488 nm laser.

In order to attempt to quantify the improvement in luminescence on the onion cells conferred by the ZnO NPs, the medium gray value on the interior of the cell of several parts of each sample and each wavelength was measured and was subtracted to the same medium value on the cell wall by using the software *ImageJ* (Annex Figure A. 12). By doing so, Table 3.6 was obtained, being possible to verify a significant increase in the fluorescence of the cell wall with the use of ZnO NPs, especially when doped with Eu. However, care should be taken when analyzing this data due to the observed differences in fluorescence between samples of the same type.

Table 3.6 –Quantification of the luminescence conferred by different FPs to the onion cells, from the images in Figure 3.16. Between parentheses, the increase in fluorescence of each FP can be observed using as a unit the value of the control image.

	Without NPs	**0% mol. Eu.**	**5% mol. Eu.**	**10% mol. Eu.**	**FITC**
405 nm laser	15 ± 4 (1)	74 ± 22 (x5.0)	85 ± 6 (x5.7)	118 ±27 (x7.9)	124 ± 7 (x8.4)
488 nm laser	8 ± 1 (1)	9 ± 3 (x1.1)	23 ± 1 (x2.9)	65 ± 8 (x8.3)	60 ± 2 (x7.6)
555 nm laser	35 ± 1 (1)	6 ± 4 (x0.2)	33 ± 11 (x1)	27 ± 5 (x0.8)	-

By analyzing Table 3.6, it is also possible to observe that FITC does not appear to produce higher fluorescence than the 10% mol. Eu ZnO NPs which was clearly visible when using lower laser intensities. One possible explanation for this is that the high intensity created by both samples may have reached a value close to the maximum to be distinguishable through this technique.

So, by analyzing Table 3.6 and Figure 3.16 is possible to conclude that the europium doped ZnO NPs present higher fluorescence compared with the undoped ZnO NPs. To verify that the luminescence did not appear only due to the europium, an experiment using only europium was also done, not showing better results than the ZnO NPs (Annex Figure A. 13). In order to do this, a small amount of europium was placed in water, shaken and placed in the onion cells.

To check if the same improvement on fluorescence, when using the Eu dopped ZnO NPs, was also observed on other cells, human cheek squamous epithelial cells were used. The results can be observed in figure 3.17.

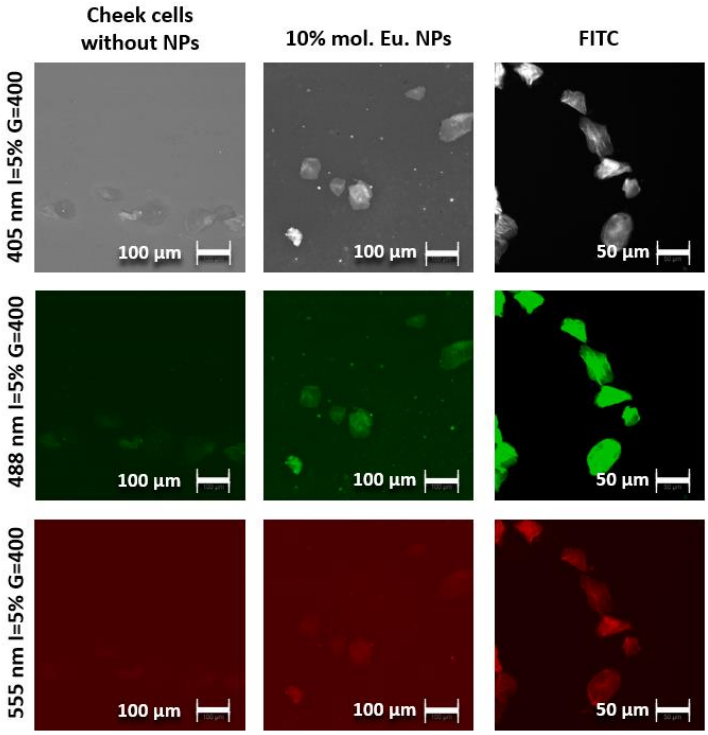

Figure 3.17 - Variation on the fluorescence intensity of cheek cells, from the left to right the column, without ZnO NPs, with 10 % mol. Eu ZnO or FITC, when irradiated with different laser excitations (top line - wavelength of 405 nm, intensity of 0.25 mW and gain of 400; middle line – wavelength of 488 nm intensity of 0.5 mW and gain of 400; bottom line wavelength of 555 nm, intensity of 0.5 mW and gain of 400).

As can be seen in Figure 3.17, when cheek cells were used, it was also verified an increase in fluorescence when using the ZnO NPs, even though these samples were more difficult to prepare. However, unlike with the onion cells, with the cheek cells, all the tested wavelengths resulted in an improvement in fluorescence.

The comparison between the use of doped ZnO NPs and the use of FITC to increase the fluorescence of the cells was also made, being verified a much higher fluorescence when FITC was used than when the same was tested with onion cell. This difference in fluorescence when using FITC on cheek cells may also be attributed to other parameters like a higher cellular uptake since FITC has a much smaller size than the NPs. In addition to this, dimethyl sulfoxide (the solute for FITC) also appeared to have some fluorescence.

Besides directly comparing the fluorescence between FITC and the ZnO NPs, other properties were also compared, such as the propensity to occur photobleaching since, when compared with traditional organic fluorescent dyes, semiconductor nanocrystals have shown high stability against photobleaching [30]. So, samples of onion with either FITC or ZnO 10 % mol. Eu. NPs were irradiated with a laser of 488 nm (most commonly used to observe fluorescence on FITC) [71].

By doing so, even though, for low laser intensities no photobleaching was observed on neither of the samples, after applying the laser at an intensity of 6 mW for 45 min, it is clear that both samples presented some photobleaching.

The photobleaching was particularly well observed on the sample with FITC, where the separation between the part of the sample that was irradiated with the laser and the part that was not is more evident than the sample that used the ZnO NPs, as can be seen in Figure 3.18 (being necessary to use higher laser intensity to observe this difference on the ZnO NPs).

In this way, ZnO NPs seem to be less prone to photobleaching, allowing their use for longer amounts of time at higher laser intensities. However, even after the irradiation of the samples and the higher photobleaching on the FITC sample, FITC still presented higher fluorescence than ZnO NPs (Annex Figure A. 14).

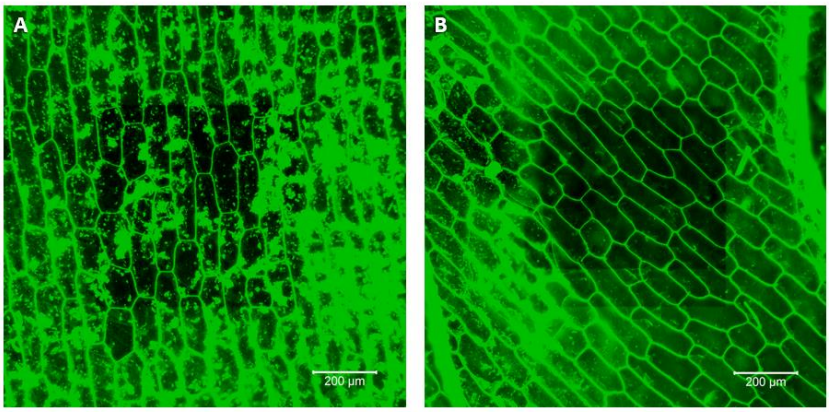

Figure 3.18 – Photobleaching effect on 10 % mol. Eu. ZnO NPs (A) and on FITC (B) when using a laser wavelength of 488 nm and an intensity of 6 mW for 45 min. Images obtained when using the same wavelength, a gain of 400, and intensity of either 6 mW (A) or 0.2 mW (B).

Another way to study the degradation of the optical properties of the samples was through the analyses of how these FPs lost their intensity over time while in solution. To do so, confocal images of the samples with the prepared solutions were taken on the day that these were prepared and after three weeks, being the solutions stored at room temperature and protected from direct sunlight. After three weeks, neither of the prepared solutions presented any deterioration of their fluorescence. The samples were then exposed to harsher conditions, being exposed to direct sunlight for a few hours a day for three days since ZnO NPs have been shown to present good stability against sunlight [30].

As can be seen in Figure 3.19, it was possible to verify that, while FITC revealed high quenching after sunlight exposure, this was not observed for the ZnO NPs. However, after sun exposure, the ZnO NPs had less stability on water, being visible a higher aggregation of these.

Even though no decrease in fluorescence was observed for the NPs not exposed to sunlight, tests over more extended periods of time could be of interest to verify the stability of each sample.

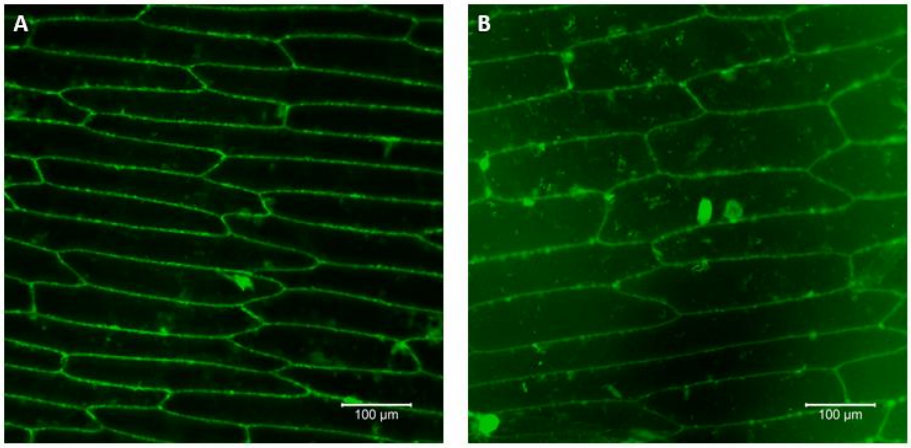

Figure 3.19 – Effect of sun light exposure on the fluorescence of 10% mol. Eu doped ZnO NPs (A) and FITC (B) on onion cells.

3.3 Cost analyses of ZnO NPs synthesis

To finalize, the cost production of the ZnO NPs was compare with the cost of FITC. It was verified that the production of 100 mg of ZnO NPs (without Eu.) has a cost of approximately 0.9 € (considering only the cost of the used chemicals) corresponding 96% of this value to the use of methanol and, have a cost of 11.8 € when doped with 10% Eu. In this way, Eu doped ZnO NPs produced through this method have a lower price, when compared with the commercial fluorophore FITC, which has a cost of 20 € or 40 €/100 mg (when bought in a quantity of 5 g or 0.1 g, respectively), becoming even more expensive when considering that FITC preferentially uses dimethyl sulfoxide instead of water as solvent (which increases its cost). However, in addition to showing better optical properties, FITC solutions can also be used with lower concentrations obtaining good results. Nevertheless, as previously noted, the cost of production of the ZnO NPs has the potential to be much lower by using other methods, not to mention the great cost reduction that can be achieved by making large-scale production.

4. Conclusions and Future Perspectives

There are many different types of FPs, presenting each one different advantages and disadvantages. In this way, ZnO NPs may be a valuable alternative to conventional FPs due to their features.

Throughout this work, several different syntheses and parameters were experimented in order to obtain ZnO NPs with the morphological and optical properties needed for the use of these on confocal microscopy. By doing so, it was possible to obtain NPs with satisfactory properties through a precipitation/microwave-assisted solvothermal method using sodium hydroxide and zinc acetate as precursors and methanol and water as solvents. Europium nitrate was also used to dope the ZnO NPs to improve their luminescence properties.

With this synthesis, it was possible to obtain spherical NPs with diameters ranging mainly from 20 to 100 nm, being their sizes controllable with the amount/concentration of ethanol and of the used precursor (NaOH). Their size, in its turn, seems to have affected the crystalline size (which has varied between the values of 15 and 55 nm) and band gap (varied between the values of 3.21 and 3.26 eV) of the NPs. Therefore, smaller NPs have smaller crystalline size and lower band gap. Some of the samples were also submitted to annealing, which led to a red-shift on the emission of these NPs when excited with a wavelength of 325 nm and also seems to favour the ion optical activation (of the europium doped NPs).

The incorporation of europium on the ZnO lattice was studied through the use of several techniques (such as XRD, EDXS, and fluorescence spectroscopy), and even though none of them can indicate without a doubt where the europium has become localized, it was possible to verify that no new crystalline structures were created (after doping the ZnO with europium). It was also noted that europium seems to be well distributed on the ZnO NPs, and that europium seemed to be located in the inter-grain space and on the surface of nanoparticles. Another relevant aspect is that EDXS has indicated that the amount of europium present on the ZnO NPs might be much smaller than the expected and thus, by using more efficient methods to dope the ZnO with Eu, the amount of Eu used to obtain the same results can be decreased.

Regarding the morphological properties of the Eu doped ZnO NPs, some of these seemed to have changed their morphology, presenting a bigger dimension when doped with europium (however, this was not observed on all samples).

The optical properties of the ZnO NPs were also analyzed, being verified that most of the samples presented significant differences on the PL and PLE spectra when doped with europium. The main differences observed were the presence of peaks associated with the europium intraionic transitions and higher emission and absorbance of longer wavelengths when doped with europium. However, when the band gap of the NPs was analysed, it was not observed major differences, being only verified an increase in the band gap of the NPs doped with europium that also presented higher dimensions. Nevertheless, other tested syntheses have also presented significant differences (to the undoped NPs produced by the main method) even without the use of europium.

A more in deep study can be done to analyse how different syntheses/methods can also affect the fluorescence of the ZnO NPs without the use of dopants and by using different solvents, which could allow to obtain these NPs through more environmentally friendly methods and allow to reduce the production cost of ZnO NPs (with high fluorescence). The reduction of production cost can also be obtained by studying ways to improve the efficiency of europium doping. As an example of this, in future works, further tests could be done on sample J (0.6 mol NaOH RT 4% mol Eu.) to better evaluate its fluorescent properties due to its good results on the steady-state macro-PL spectroscopies analysis.

The comparison between the fluorescence of different syntheses, however, presents the challenge that the intensity of emission is usually given in arbitrary units, being difficult to compare different studies on literature.

Still regarding the optical properties of the ZnO NPs, some of the produced NPs were tested on onion and human cheek cells by using confocal microscopy. By doing so, it was verified a significant increase in the fluorescence of the cells conferred by the NPs, especially when the NPs were doped with europium. The produced ZnO NPs were directly compared with a common commercially available fluorophore (FITC). It was observed that although the latter presents higher fluorescence intensities, it suffers from more damage when subjected to sun exposure and appeared to be more prone to photobleaching than the ZnO NPs.

Another aspect that could be of interest to study is the toxicity of these NPs and how selective these NPs are toward different cells. In particular, between healthy and cancer cells since, for instance, ZnO NPs have been reported to present anti-cancer properties and thanks to their fluorescence, the higher selectivity of these NPs towards cancer cells could be directly observed/studied by using fluorescence microscopy.

To finalize, through this work, it was possible to increase the luminescence of ZnO NPs for longer wavelengths than U.V. and even though the use of ZnO NPs on biological samples still present several challenges, due to the advantages mentioned above (which are not present in most of the other PFs) ZnO NPs may have a bright future on bioimaging and theragnostic, helping to find better ways to study and combat diseases.

References

[1] A. K. Barui, R. Kotcherlakota, and C. R. Patra, *Biomedical applications of zinc oxide nanoparticles*. Elsevier Inc., pp. 258-260, 2018, doi: 10.1016/B978-0-12-813661-4.00006-7.

[2] D. J. Stephens, V. J. Allan, and D. J. S. and V. J. Allan, "Light Microscopy Techniques for Live Cell Imaging," *Am. Assoc. Adv. Sci.*, vol. 300, no. 5616, pp. 82–86, 2016.

[3] M. J. Sanderson *et al.*, "Fluorescence Microscopy," *Cold Spring Harb. Protoc.*, vol. 2014, no. 10, pp. 1042-1065, Oct. 2014, doi: 10.1101/pdb.top071795.

[4] M. Weigert *et al.*, "Content-aware image restoration: pushing the limits of fluorescence microscopy," *Nat. Methods*, pp. 1091-1097, 2018, doi: 10.1038/s41592-018-0216-7.

[5] J. S. PLOEM, "Fluorescence Microscopy," in *Fluorescent and Luminescent Probes for Biological Activity*, Elsevier, pp. 3–13, 1999, doi: 10.1016/B978-012447836-7/50003-8.

[6] G. Paës, "Fluorescent probes for exploring plant cell wall deconstruction: A review," *Molecules*., pp. 9380-9398 2014. doi: 10.3390/molecules19079380.

[7] S. Verbrugge, L. C. Kapitein, and E. J. G. Peterman, "Kinesin moving through the spotlight: Single-motor fluorescence microscopy with submillisecond time resolution," *Biophys. J.*, pp. 2536-2546, 2007, doi: 10.1529/biophysj.106.093575.

[8] "Fluorescent Probes | Thermo Fisher Scientific - PT." https://www.thermofisher.com/pt/en/home/life-science/protein-biology/protein-biology-learning-center/protein-biology-resource-library/pierce-protein-methods/fluorescent-probes.html (accessed Oct. 20, 2020).

[9] G. G. Guilbault, "Practical Fluorescence. Modern Monographs in Analytical Chemistry," *CRC Press*, pp. 1–40, 1990.

[10] "What is the difference between fluorescence phosphorescence and luminescence? - Enzo Life Sciences." https://www.enzolifesciences.com/science-center/technotes/2019/december/what-is-the-difference-between-fluorescence-phosphorescence-and-luminescence?/ (accessed Oct. 20, 2020).

[11] S. W. Paddock, "Principles and practices of laser scanning confocal microscopy," *Applied Biochemistry and Biotechnology - Part B Molecular Biotechnology*., pp. 127-149, 2000. doi: 10.1385/mb:16:2:127.

[12] A. Nwaneshiudu, C. Kuschal, F. H. Sakamoto, R. Rox Anderson, K. Schwarzenberger, and R. C. Young, "Introduction to confocal microscopy," *J. Invest. Dermatol.*, pp. 1-4, 2012, doi: 10.1038/jid.2012.429.

[13] "Confocal Laser Scanning Microscope." https://www.cenimat.fct.unl.pt/sites/www.cenimat.fct.unl.pt/files/Flyers/Confocal_flyer_v1.0.pdf (accessed Nov. 29, 2020).

[14] J. Lakowicz, *Principles of fluorescence spectroscopy*, 2nd ed. Kluwer Academic/Plenum Publishers, pp. 1-94 1999.

[15] B. Hötzer, I. L. Medintz, and N. Hildebrandt, "Fluorescence in nanobiotechnology: Sophisticated fluorophores for novel applications," *Small*., pp. 1-24, 2012. doi: 10.1002/smll.201200109.

[16] D. Jin, P. Xi, B. Wang, L. Zhang, J. Enderlein, and A. M. Van Oijen, "Nanoparticles for super-resolution microscopy and single-molecule tracking," *Nature Methods*., pp. 415-423, 2018. doi: 10.1038/s41592-018-0012-4.

[17] B. A. Kairdolf, X. Qian, and S. Nie, "Bioconjugated nanoparticles for biosensing, in vivo imaging, and medical diagnostics," *Analytical Chemistry*., pp. 1015-1031, 2017. doi: 10.1021/acs.analchem.6b04873.

[18] F. W. Pratiwi, C. W. Kuo, B. C. Chen, and P. Chen, "Recent advances in the use of fluorescent nanoparticles for bioimaging," *Nanomedicine*, pp. 1759-1769, 2019, doi: 10.2217/nnm-2019-0105.

[19] O. S. Wolfbeis, "An overview of nanoparticles commonly used in fluorescent bioimaging," *Chemical Society Reviews*., pp. 4743-4768, 2015. doi: 10.1039/c4cs00392f.

[20] I. M. Adjei, B. Sharma, and V. Labhasetwar, "Nanoparticles: Cellular uptake and cytotoxicity," *Adv. Exp. Med. Biol.*, pp. 73-91, 2014, doi: 10.1007/978-94-017-8739-0_5.

[21] J. E. Eixenberger *et al.*, "Defect Engineering of ZnO Nanoparticles for Bioimaging Applications," *ACS Appl. Mater. Interfaces*, pp. 24933-24944, 2019, doi: 10.1021/acsami.9b01582.

[22] M. K. Patra *et al.*, "Synthesis of stable dispersion of ZnO quantum dots in aqueous medium showing visible emission from bluish green to yellow," *J. Lumin.*, pp. 320–324, 2009, doi: 10.1016/j.jlumin.2008.10.014.

[23] J. Jiang, J. Pi, and J. Cai, "The Advancing of Zinc Oxide Nanoparticles for Biomedical Applications," *Bioinorg. Chem. Appl.*, vol. 2018, pp. 1-18, 2018, doi: https://doi.org/10.1155/2018/1062562.

[24] S. Sruthi, J. Ashtami, and P. V. Mohanan, "Biomedical application and hidden toxicity of Zinc oxide nanoparticles," *Materials Today Chemistry*. pp. 258–260, 2018. doi: 10.1016/j.mtchem.2018.09.008.

[25] M. K. Patra *et al.*, 'Synthesis of stable dispersion of ZnO quantum dots in aqueous medium showing visible emission from bluish green to yellow,' vol. 129, pp. 320–324, 2009, doi: 10.1016/j.jlumin.2008.10.014.

[26] H. Agarwal, S. V. Kumar, and S. Rajeshkumar, "A review on green synthesis of zinc oxide nanoparticles – An eco-friendly approach," *Resour. Technol.*, vol. 3, no. 4, pp. 406–413, 2017, doi: 10.1016/j.reffit.2017.03.002.

[27] A. Pimentel *et al.*, "Effect of solvents on ZnO nanostructures synthesized by solvothermal method assisted by microwave radiation: a photocatalytic study," *J. Mater. Sci.*, pp. 5777-5787, 2015, doi: 10.1007/s10853-015-9125-7.

[28] L. Irimpan, V. P. N. Nampoori, P. Radhakrishnan, A. Deepthy, and B. Krishnan, "Size dependent fluorescence spectroscopy of nanocolloids of ZnO," *J. Appl. Phys.*, pp. 1-6, 2007, doi: 10.1063/1.2778637.

[29] Z. Y. Zhang and H. M. Xiong, "Photoluminescent ZnO nanoparticles and their biological applications," *Materials (Basel).*, pp. 3102-3127, 2015, doi: 10.3390/ma8063101.

[30] H. M. Xiong, "ZnO nanoparticles applied to bioimaging and drug delivery," *Adv. Mater.*, pp. 5329-5335, 2013, doi: 10.1002/adma.201301732.

[31] N. Goswami and D. K. Sharma, "Structural and optical properties of unannealed and annealed ZnO nanoparticles prepared by a chemical precipitation technique," *Phys. E Low-Dimensional Syst. Nanostructures*, pp. 1675-1682, 2010, doi: 10.1016/j.physe.2010.01.023.

[32] Z. Zhang and H. Xiong, "Photoluminescent ZnO Nanoparticles and Their Biological Applications," *Materials (Basel).*, pp. 3101–3127, 2015, doi: 10.3390/ma8063101.

[33] H. M. Xiong, "Photoluminescent ZnO nanoparticles modified by polymers," *J. Mater. Chem.*, pp. 4251-4262, 2010, doi: 10.1039/b918413a.

[34] M. Carofiglio, S. Barui, V. Cauda, and M. Laurenti, “Doped zinc oxide nanoparticles: Synthesis, characterization and potential use in nanomedicine,” *Applied Sciences (Switzerland).*, pp. 1-43, 2020. doi: 10.3390/app10155194.

[35] P. M. Aneesh and M. K. Jayaraj, “Red luminescence from hydrothermally synthesized Eu-doped ZnO nanoparticles under visible excitation,” *Bull. Mater. Sci.*, pp. 227–231, 2010, doi: 10.1007/s12034-010-0035-7.

[36] M. Peres *et al.*, “Optical studies of ZnO nanocrystals doped with Eu3+ ions,” *Appl. Phys. A Mater. Sci. Process.*, pp. 129–133, 2007, doi: 10.1007/s00339-007-3941-9.

[37] Y. Liu, W. Luo, R. Li, G. Liu, M. R. Antonio, and X. Chen, “Optical spectroscopy of Eu3+ doped ZnO nanocrystals,” *J. Phys. Chem. C*, pp. 686–694, 2008, doi: 10.1021/jp077001z.

[38] J. Kaszewski *et al.*, “Tuning the luminescence of ZnO:Eu nanoparticles for applications in biology and medicine,” *Opt. Mater. (Amst).*, pp. 77-86, 2018, doi: 10.1016/j.optmat.2018.04.028.

[39] M. Gerigk *et al.*, “Nanoparticle shape anisotropy and photoluminescence properties: Europium containing ZnO as a Model Case,” *Nanoscale*, pp. 1-12, 2015, doi: 10.1039/c5nr02550h.

[40] K. Suzuki, K. Murayama, and N. Tanaka, “Enhanced luminescence in Eu-doped ZnO nanocrystalline films,” *Appl. Phys. Lett.*, pp. 1-4, 2015, doi: 10.1063/1.4926986.

[41] M. Samadi, M. Zirak, A. Naseri, E. Khorashadizade, and A. Z. Moshfegh, “Recent progress on doped ZnO nanostructures for visible-light photocatalysis,” *Thin Solid Films*., pp.2-19, 2016. doi: 10.1016/j.tsf.2015.12.064.

[42] B. Ghaemi, O. Mashinchian, T. Mousavi, R. Karimi, S. Kharrazi, and A. Amani, “Harnessing the Cancer Radiation Therapy by Lanthanide-Doped Zinc Oxide Based Theranostic Nanoparticles,” *ACS Appl. Mater. Interfaces*, pp. 3123–3134, 2016, doi: 10.1021/acsami.5b10056.

[43] J. Huang *et al.*, “Synthesis and optical properties of Eu3+ doped ZnO nanoparticles used for white light emitting diodes,” *J. Nanosci. Nanotechnol.*, pp. 3052-3055, 2014, doi: 10.1166/jnn.2014.8620.

[44] B. Ş. Vasile *et al.*, “Eu3+-doped ZnO nanostructures: Advanced characterizations, photoluminescence and cytotoxic effect,” *Rom. J. Morphol. Embryol.*, pp. 941-952, 2017.

[45] J. Lian, Y. Liang, F. L. Kwong, Z. Ding, and D. H. L. Ng, “Template-free solvothermal synthesis of ZnO nanoparticles with controllable size and their size-dependent optical properties,” *Mater. Lett.*, pp. 318-320, 2012, doi: 10.1016/j.matlet.2011.09.007.

[46] D. Sharma, S. Sharma, B. S. Kaith, J. Rajput, and M. Kaur, “Synthesis of ZnO nanoparticles using surfactant free in-air and microwave method,” *Appl. Surf. Sci.*, pp. 9661-9672, 2011, doi: 10.1016/j.apsusc.2011.06.094.

[47] S. M. Saleh, “ZnO nanospheres based simple hydrothermal route for photocatalytic degradation of azo dye,” *Spectrochim. Acta - Part A Mol. Biomol. Spectrosc.*, pp. 141-147, 2019, doi: 10.1016/j.saa.2018.11.065.

[48] A. Asok, A. R. Kulkarni, and M. N. Gandhi, “Microwave accelerated one-minute synthesis of luminescent ZnO quantum dots,”, pp. 404-405, 2013. doi: 10.1063/1.4791082.

[49] H. Agarwal, S. V. Kumar, S. Rajeshkumar, S. Venkat Kumar, and S. Rajeshkumar, “A review on green synthesis of zinc oxide nanoparticles – An eco-friendly approach,” *Resour. Technol.*, vol. 3, no. 4, pp. 406–413, Dec. 2017, doi: 10.1016/j.reffit.2017.03.002.

[50] V. Koutu, L. Shastri, and M. M. Malik, “Effect of NaOH concentration on optical properties of zinc oxide nanoparticles,” *Mater. Sci. Pol.*, pp. 819 - 827, 2016, doi: 10.1515/msp-2016-0119.

[51] V. Kumar, V. Kumar, S. Som, M. M. Duvenhage, O. M. Ntwaeaborwa, and H. C. Swart, "Effect of Eu doping on the photoluminescence properties of ZnO nanophosphors for red emission applications," *Appl. Surf. Sci.*, pp. 419-430,2014, doi: 10.1016/j.apsusc.2014.04.192.

[52] J. I. Goldstein, D. E. Newbury, J. R. Michael, N. W. M. Ritchie, J. H. J. Scott, and D. C. Joy, *Scanning electron microscopy and x-ray microanalysis*., pp. 209-230, 2017. doi: 10.1007/978-1-4939-6676-9.

[53] H. Yadav, N. Sinha, S. Goel, and B. Kumar, "Eu-doped ZnO nanoparticles for dielectric, ferroelectric and piezoelectric applications," *J. Alloys Compd.*, pp. 333-341, 2016, doi: 10.1016/j.jallcom.2016.07.329.

[54] J. C. Sin, S. M. Lam, I. Satoshi, K. T. Lee, and A. R. Mohamed, "Sunlight photocatalytic activity enhancement and mechanism of novel europium-doped ZnO hierarchical micro/nanospheres for degradation of phenol," *Appl. Catal. B Environ.*, pp. 258-268, 2014, doi: 10.1016/j.apcatb.2013.11.001.

[55] M. C. Morris, H. F. McMurdie, E. H. Evans, B. Paretzkin, H. S. Parker, and N. P. Pyrros, *Standard X-ray diffraction powder patterns. Monograph 25 Section 20*. 1964.

[56] S. Dhara and A. K. Raychaudhuri, "Enhancement in red emission at room temperature from europium doped ZnO nanowires by 1,10 phenanthroline-europium interface induced resonant excitations," *AIP Adv.*, pp. 1-12, 2017, doi: 10.1063/1.4976821.

[57] J. Yang *et al.*, "Synthesis and optical properties of Eu-doped ZnO nanosheets by hydrothermal method," *Mater. Sci. Semicond. Process.*, pp. 247-252, 2011, doi: 10.1016/j.mssp.2011.04.002.

[58] J. Nanosains, "Derivation of Scherrer Relation Using an Approach in Basic Physics Course," *Nano*, pp. 28-32, 2008.

[59] B. D. Cullity and S. R. Stock, "Elements of X-ray diffraction, 3rd edition," *Prentice Hall*, 2001.

[60] Y. Zong, Z. Li, X. Wang, J. Ma, and Y. Men, "Synthesis and high photocatalytic activity of Eu-doped ZnO nanoparticles," *Ceram. Int.*, pp. 10375-10382, 2014, doi: 10.1016/j.ceramint.2014.02.123.

[61] C. M. Maguire, M. Rösslein, P. Wick, and A. Prina-Mello, "Characterisation of particles in solution–a perspective on light scattering and comparative technologies," *Science and Technology of Advanced Materials*, pp. 732–745, 2018. doi: 10.1080/14686996.2018.1517587.

[62] A. El-Denglawey, M. M. Makhlouf, and M. Dongol, "Physical aging effects on the structural and optical properties of nano As-Se-Tl films," *J. Non. Cryst. Solids*, pp. 34-40, 2016, doi: 10.1016/j.jnoncrysol.2016.07.012.

[63] P. Makuła, M. Pacia, and W. Macyk, "How To Correctly Determine the Band Gap Energy of Modified Semiconductor Photocatalysts Based on UV-Vis Spectra," *Journal of Physical Chemistry Letters*., pp. 6814-6817, 2018. doi: 10.1021/acs.jpclett.8b02892.

[64] S. Benramache, O. Belahssen, A. Guettaf, and A. Arif, "Correlation between crystallite size-optical gap energy and precursor molarities of zno thin films," *J. Semicond.*, pp. 1-4, 2014, doi: 10.1088/1674-4926/35/4/042001.

[65] S. Benramache, A. Arif, O. Belahssen, and A. Guettaf, "Study on the correlation between crystallite size and optical gap energy of doped ZnO thin film," *J. Nanostructure Chem.*, pp. 1-6, 2013, doi: 10.1186/2193-8865-3-80.

[66] R. Marin *et al.*, "Europium-doped ZnO nanosponges-controlling optical properties and photocatalytic activity," *J. Mater. Chem. C*, pp. 3909-3919, 2019, doi: 10.1039/c9tc00215d.

[67] M. Goswami, N. C. Adhikary, and S. Bhattacharjee, "Effect of annealing temperatures on the structural and optical properties of zinc oxide nanoparticles prepared by chemical precipitation method," *Optik (Stuttg).*, pp. 1006-1015, 2018, doi: 10.1016/j.ijleo.2017.12.174.

[68] J. Yang *et al.*, “Effect of annealing temperature on the structure and optical properties of ZnO nanoparticles,” *J. Alloys Compd.*, pp. 632–635, 2009, doi: 10.1016/j.jallcom.2008.10.135.

[69] N. Carpita, D. Sabularse, D. Montezinos, and D. P. Delmer, “Determination of the pore size of cell walls of living plant cells,” *Science.*, pp. 1144-1147, 1979, doi: 10.1126/science.205.4411.1144.

[70] R. Nair, S. H. Varghese, B. G. Nair, T. Maekawa, Y. Yoshida, and D. S. Kumar, “Nanoparticulate material delivery to plants,” *Plant Science*., pp. 154-163, 2010. doi: 10.1016/j.plantsci.2010.04.012.

[71] “Fluorescein (FITC) | Thermo Fisher Scientific - PT.” https://www.thermofisher.com/pt/en/home/life-science/cell-analysis/fluorophores/fluorescein.html?SID=fr-fitc-main (accessed Nov. 18, 2020).

Annexes

Annex A – Different used syntheses

- **First tested method:**

- Based on the article *"Tuning the luminescence of ZnO:Eu nanoparticles for applications in biology and medicine"*[38]:

1. Use of 24 or 20 ml of Zn(NO3)2·6H2O, 10 or 25 mM.
2. Addition of 1 or 5 ml of a 1 M solution of NaOH and the solution was stirred with a magnet.
3. The solution was placed in the microwave in a reaction vessel and heated to 140 ºC for 10 minutes with a power of 100 or 150 Watts and cooled down to 50 ºC.
4. Then precipitated product was collected to centrifuge tubes and washed twice with water and twice with IPA using 4000 rpm centrifugation for 1 minute each time.
5. The obtained nanoparticles were left to dry and then analyzed through SEM.

- **Second tested method:** This was the main method used to synthesize the ZnO NPs and is described in materials and methods.

- **Third tested method:**

- Based on the article *"*Microwave accelerated one-minute synthesis of luminescent ZnO quantum dots*"*[48]:

1. The starting precursors Zn(OAc)2 and LiOH were used as received without further purification.
2. The solvent used for synthesis was absolute ethanol.
3. In a typical synthesis, 30ml of 0.05M Zn(OAc)2 was mixed with 30ml of 0.05M LiOH in a sealed vessel under magnetic stirring.
4. The reaction was initiated by microwave irradiation with magnetic stirring.
5. The microwave power was 50 W and the solutions, with a volume of 20, 15, or 10 ml, were heated up to 75°C or 100º, and then the temperature was maintained for one or five minutes with high magnetic stirring.
6. The mixture was cooled to room temperature.

- **Forth tested method:**

- Based on the article *"ZnO nanospheres based simple hydrothermal route for photocatalytic degradation of azo dye"*[48]:

1. 16 mL of 1M or 2.1M KOH solution was mixed with 80 mL of ethylene glycol under regular and stable stirring using a magnetic stirrer.
2. Then, 16 mL of 0.4 M Zn(NO3)2.6H2O solution was added.
3. The mixture was stirred for some time.
4. Different amounts of CTAB were added to part of the obtained solution, each part of 25 ml, to monitor the nanostructure morphology of the ZnO particles.
5. This mixed solution is put in the microwave for 5 or 15 min.
6. After the reaction was accomplished, the solution was cooled, the white nanomaterial powder was centrifuged and washed several times with water and IPA and was air-dried.

- **Fifth tested method:**

- Based on the article *"Synthesis of ZnO nanoparticles using surfactant free in-air and micro-wave method"*[46] *and "Synthesis of ZnO nanoparticles and study of their antibacterial and antifungal properties"*[49]:

1. The synthesis was carried out using zinc sulphate heptahydrate and sodium hydroxide as pre-cursors. 0.1 M ZnSO47H2O and 0.4 M NaOH aqueous solutions were mixed.
2. The resulting mixture was vigorously stirred.
3. Some solutions were put in the microwave oven for 1 or 2 min.
4. The white product obtained through centrifugation was thoroughly washed with distilled water and dried in the air.

- **Sixth tested method:**

- Based on the article *"Template-free solvothermal synthesis of ZnO nanoparticles with control-lable size and their size-dependent optical properties"*[45]:

1. In a typical sample preparation, 7.5 mmol of Zn(CH3COO)2·2H2O was put into a 75 mL mixed solutions of anhydrous ethanol and ethylene glycol (EG), with a volume ratio of 50:25 ml.
2. The mixture was stirred to form a homogenous solution and then transferred into a microwave and heated at 140 °C or 100°C for 10 or 20 min.
3. The solution was cooled to room temperature. The products were collected and washed with deionized water and IPA before being air-dried.

- **Seventh tested method:**

- Based on the article *"Synthesis of stable dispersion of ZnO quantum dots in aqueous medium showing visible emission from bluish green to yellow"*[22]:

1. In a typical synthesis, 0.1 M zinc acetate solution by dissolving 0.55 g of zinc acetate in 25 ml of methanol and 1 M KOH solution by dissolving 2.8 g of KOH in 50 ml methanol were prepared separately.
2. The reaction was carried out at room temperature by dropwise addition of KOH solution to zinc acetate solution with constant stirring.
3. The final pH of the solution was maintained at 10.
4. The resulting solution was homogenized by stirring continuously for 1 h with a magnetic stirrer.
5. The solution obtained was found to show bright bluish-green luminescence under UV excitation, thereby indicating the formation of ZnO particles.
6. At this stage, 0.25 ml of tetraethylorthosillicate (TEOS) solution (98%, ACROS, USA) was added to the ZnO solution to control particle growth.
7. Immediately after this, 0.5 ml of distilled water was injected into the colloidal solution for mild sol-gel reaction of silica on particle surfaces.
8. The as-prepared colloid was separated by centrifuging and washed several times by methanol followed by distilled water to remove unreacted molecules.

- **Eighth tested method:**

- Based on the article *"*Defect Engineering of ZnO Nanoparticles for Bioimaging Applications*"*[21]:

1. 1 g of Zinc acetate dihydrate was used as the zinc source and 50 ml diethylene glycol (DEG) as the solvent.
2. 2 g of polyvinylpyrrolidone (PVP) were added to the previous solution and the solution was heated to 80 ºC being 0.5 ml of water added afterward and the solution was re-heated to 150 ºC.
3. Once the solution cooled to room temperature, the samples were centrifuged and washed with water and IPA.
4. After being dried, the NPs were annealed in air at temperatures of 550 ºC.

Annex B – Additional figures

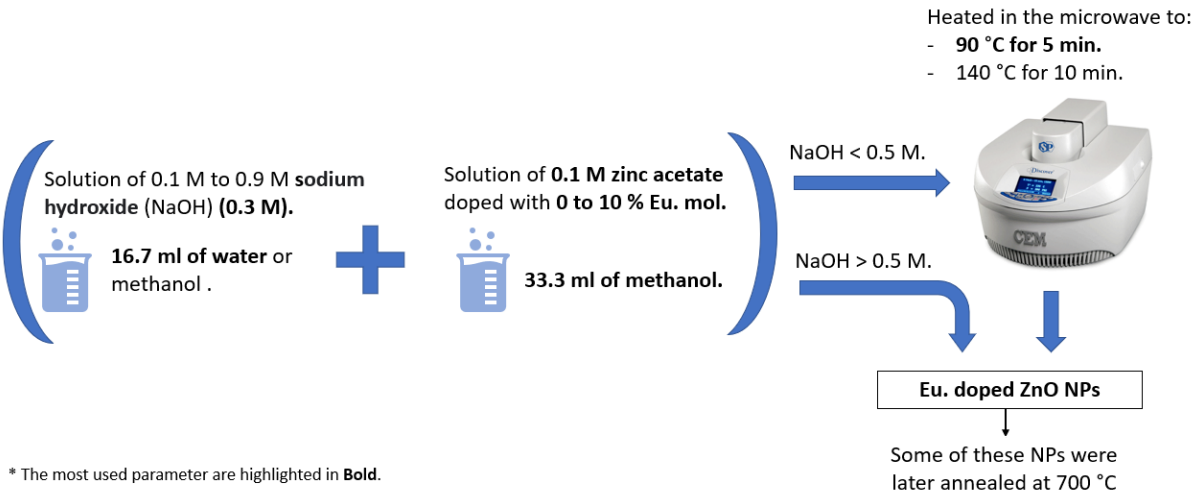

Annex Figure A. 1 – Schematic of the ZnO synthesis by the main method used throughout this dissertation.

Annex Figure A. 2 - Preparation of the onion cells on the microscope slide.

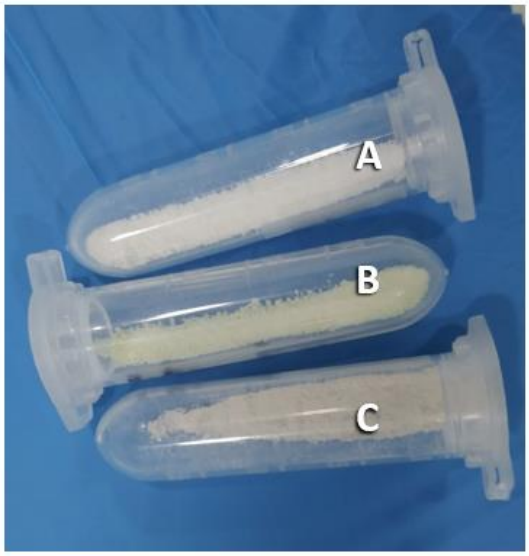

Annex Figure A. 3 – Different colors between the samples not annealed and annealed; A – Sample unannealed, B and C – Samples annealed.

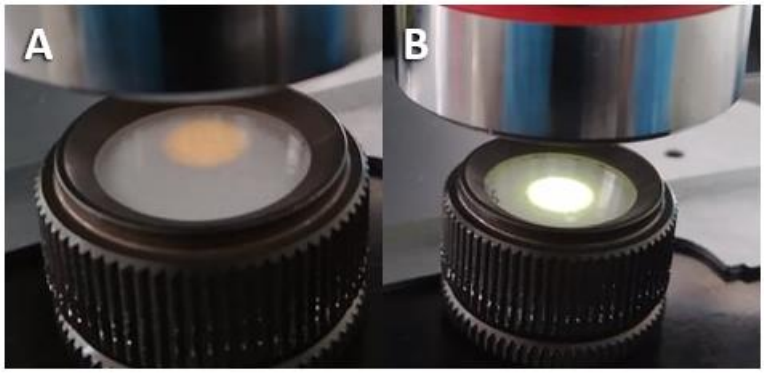

Annex Figure A. 4 – Observable fluorescence of the ZnO NPs when submitted to U.V. radiation; A – Represents the fluorescence visualized on most samples, B – NPs obtained by method 7.

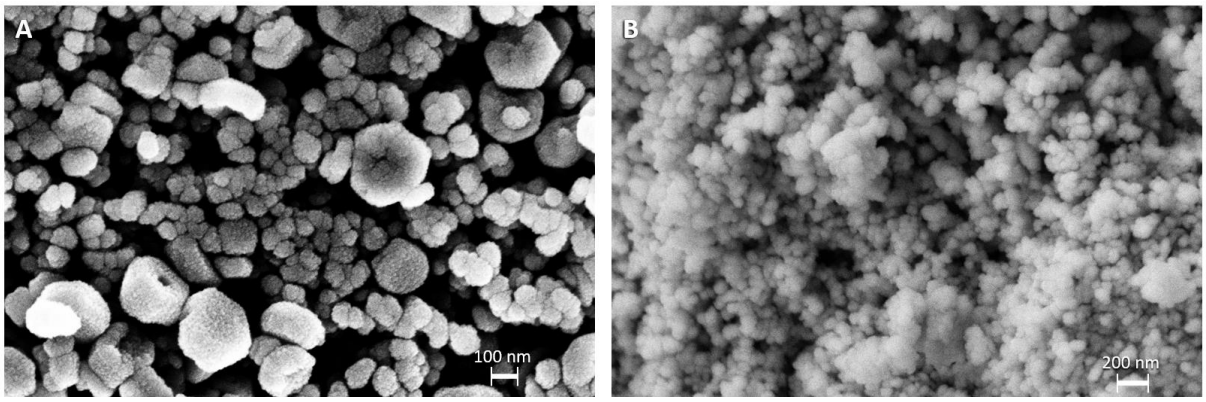

Annex Figure A. 5 - A) ZnO NPs 5% mol. Eu. B) ZnO NPs 0.6 mol. NaOH RT 4%mol.Eu.

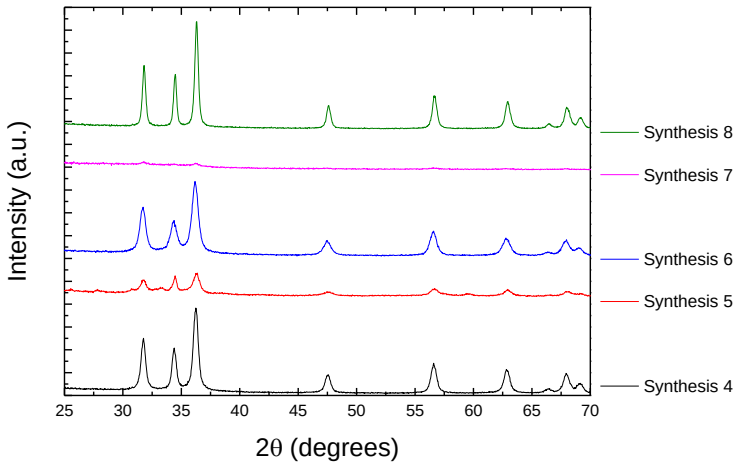

Annex Figure A. 6 – DRX diffractograms obtained for the syntheses 4, 5, 6, 7, and 8. Even though the ZnO peaks are not well observed on synthesis 7 this was identified as ZnO.

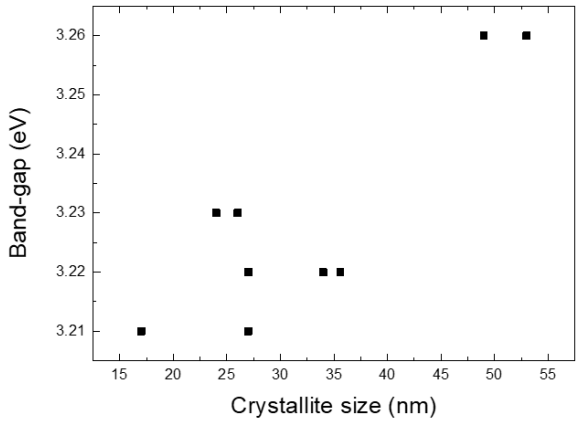

Annex Figure A. 7 - Variation of the band gap with the crystallite size for the NPs produced by the main method (including the annealed NPs).

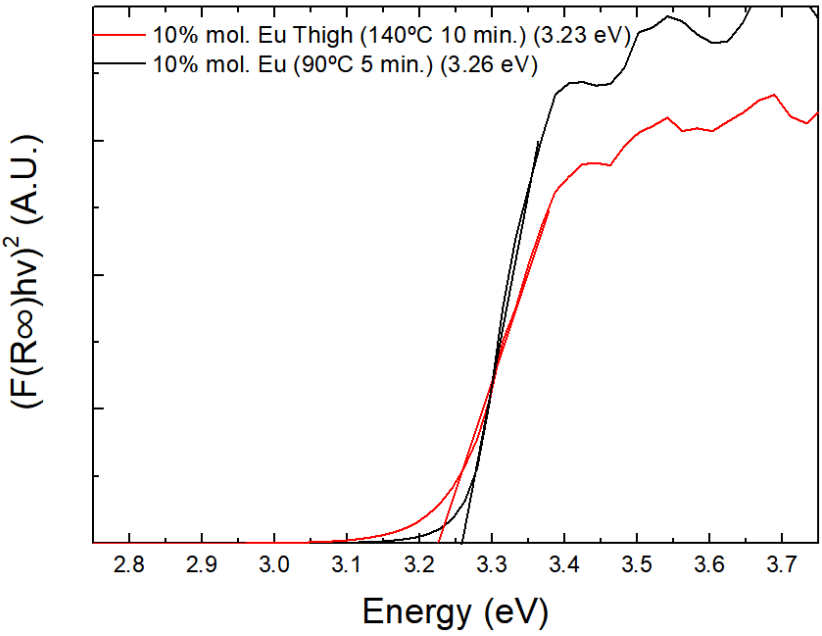

Annex Figure A. 8 - Graphs obtained for the band gap calculation of the samples doped with 10% mol. Eu when used different microwave time and temperatures.

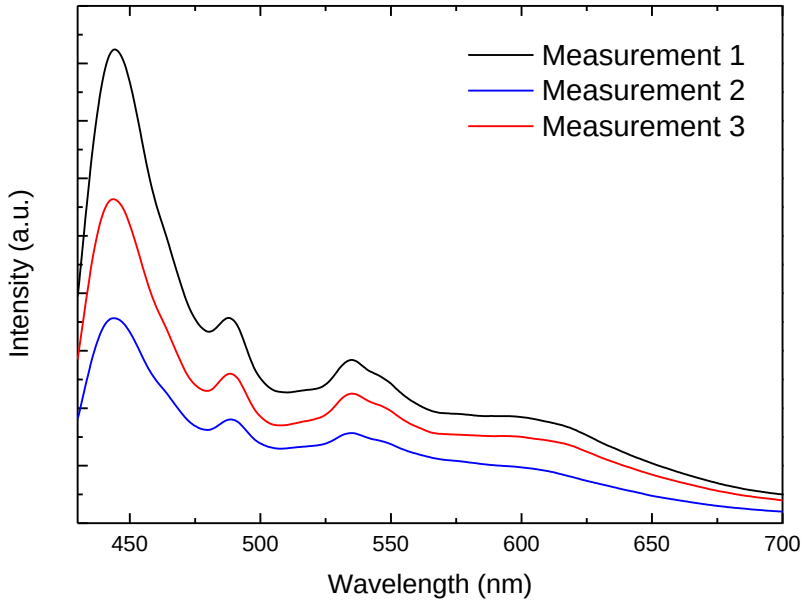

Annex Figure A. 9 – Variations on the fluorescence intensity of the ZnO NPs obtained between different measures of the same tested sample (10% mol. Eu).

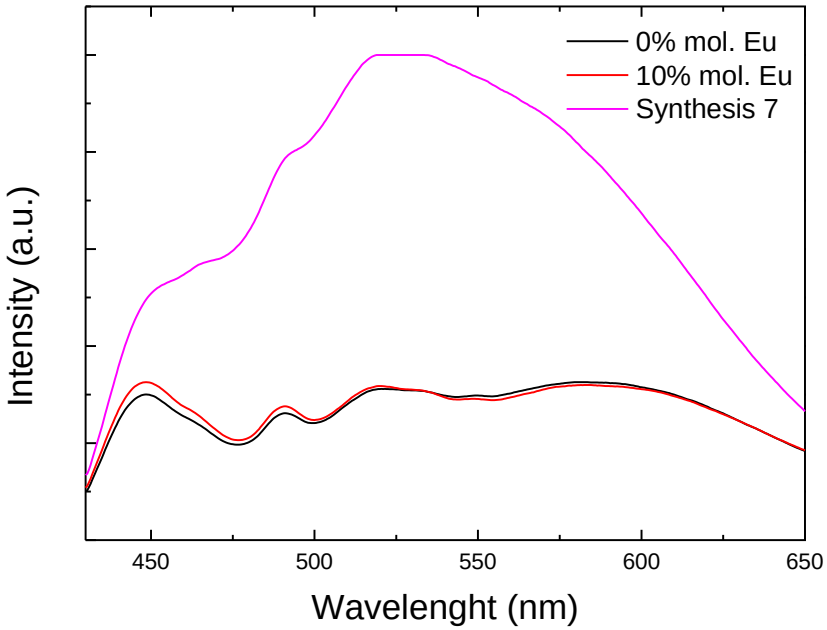

Annex Figure A. 10 – Different intensities obtained for the NPs produced by the main used synthesis and synthesis 7 for an excitation wavelength of 380 nm.

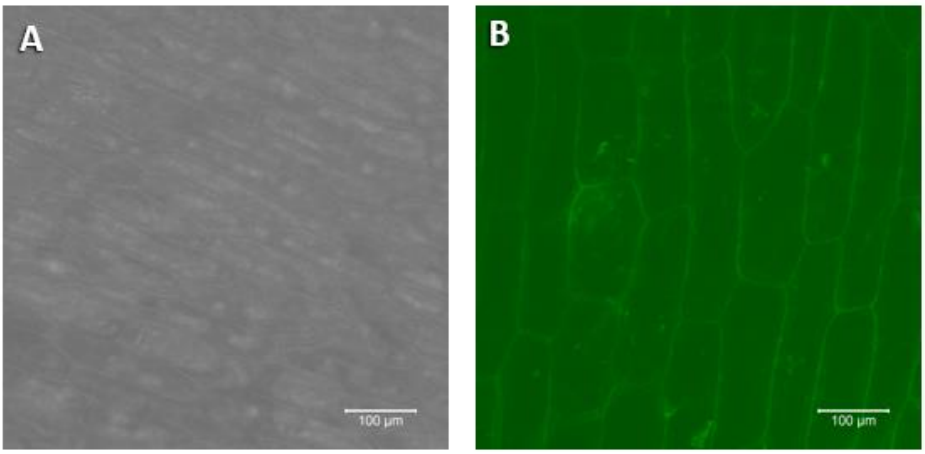

Annex Figure A. 11 – Comparison between the fluorescence of the 10% mol. Eu ZnO NPs when used a 405 nm laser (A) and a 488 nm laser (B) with 0.05 mW.

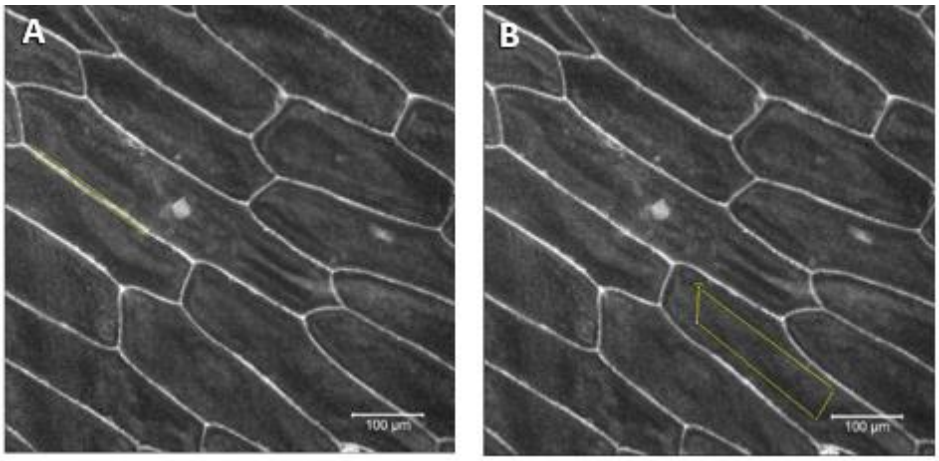

Annex Figure A. 12 – Illustrative figures of how the medium gray values on the cell wall (A) and interior of the cell (B) were done.

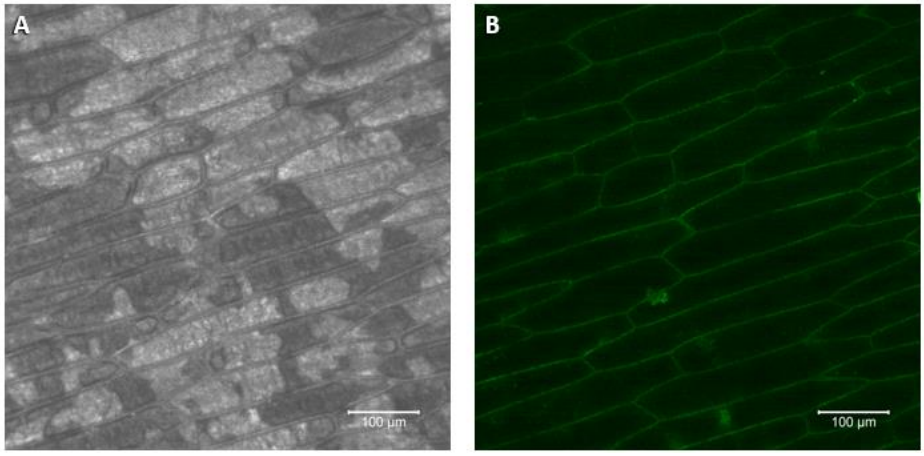

Annex Figure A. 13 – Fluorescence observed when used a suspension of europium in water instead of the Eu doped NPs on the onion cells when using a laser of 405 nm at 2% (A) or a laser of 488 nm at 2% (B).

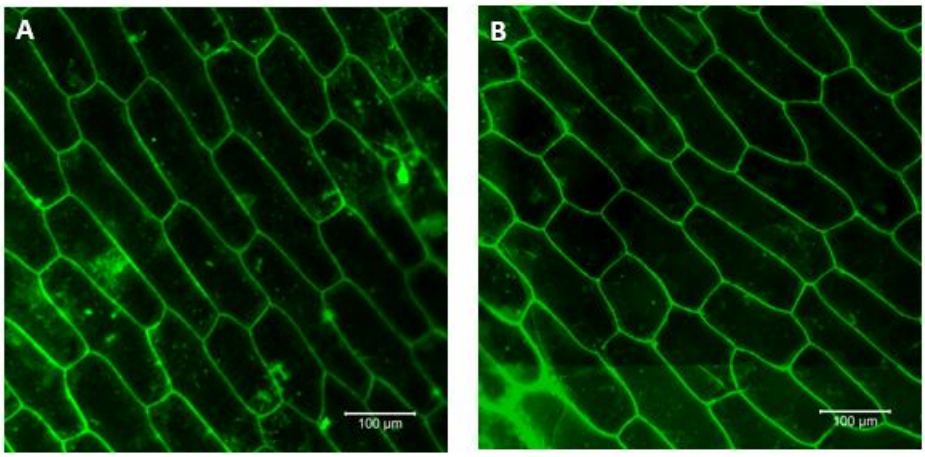

Annex Figure A. 14 – Comparison between the use of 10% mol. Eu doped ZnO NPs without photobleaching (A) and FITC after being exposed to the 488 laser for 45 min. (B).